frontiers in Earth Science

ORIGINAL RESEARCH
published: 28 May 2021
doi: 10.3389/feart.2021.671401

Holocene Spatiotemporal Redox Variations in the Southern Baltic Sea

Dalton S. Hardisty[1], Natascha Riedinger[2], Noah J. Planavsky[3], Dan Asael[3], Steven M. Bates[4] and Timothy W. Lyons[4]*

[1] Department of Earth and Environmental Sciences, Michigan State University, East Lansing, MI, United States, [2] Boone Pickens School of Geology, Oklahoma State University, Stillwater, OK, United States, [3] Department of Geology and Geophysics, Yale University, New Haven, CT, United States, [4] Department of Earth and Planetary Sciences, University of California, Riverside, Riverside, CA, United States

Low oxygen conditions in the modern Baltic Sea are exacerbated by human activities; however, anoxic conditions also prevailed naturally over the Holocene. Few studies have characterized the specific paleoredox conditions (manganous, ferruginous, euxinic) and their frequency in southern Baltic sub-basins during these ancient events. Here, we apply a suite of isotope systems (Fe, Mo, S) and associated elemental proxies (e.g., Fe speciation, Mn) to specifically define water column redox regimes through the Baltic Holocene in a sill-proximal to sill-distal transect (Lille Belt, Bornholm Basin, Landsort Deep) using samples collected during the Integrated Ocean Drilling Program Expedition 347. At the sill-proximal Lille Belt, there is evidence for anoxic manganous/ferruginous conditions for most of the cored interval following the transition from the Ancylus Lake to Littorina Sea but with no clear excursion to more reducing or euxinic conditions associated with the Holocene Thermal Maximum (HTM) or Medieval Climate Anomaly (MCA) events. At the sill-distal southern sub-basin, Bornholm Basin, a combination of Fe speciation, pore water Fe, and solid phase Mo concentration and isotope data point to manganous/ferruginous conditions during the Ancylus Lake-to-Littorina Sea transition and HTM but with only brief excursions to intermittently or weakly euxinic conditions during this interval. At the western Baltic Proper sub-basin, Landsort Deep, new Fe and S isotope data bolster previous Mo isotope records and Fe speciation evidence for two distinct anoxic periods but also suggest that sulfide accumulation beyond transient levels was largely restricted to the sediment-water interface. Ultimately, the combined data from all three locations indicate that Fe enrichments typically indicative of euxinia may be best explained by Fe deposition as oxides following events likely analogous to the periodic incursions of oxygenated North Sea waters observed today, with subsequent pyrite formation in sulfidic pore waters. Additionally, the Mo isotope data from multiple Baltic Sea southern basins argue against restricted and widespread euxinic conditions, as has been demonstrated in the Baltic Proper and Bothnian Sea during the HTM or MCA. Instead, similar to today, each past Baltic anoxic event is characterized by redox conditions that become progressively more reducing with increasing distance from the sill.

Keywords: Baltic Sea, paleoredox, diagenesis, molybdenum isotopes, iron isotopes, sulfur isotopes, IODP Expedition 347

OPEN ACCESS

Edited by:
Paolo Censi,
University of Palermo, Italy

Reviewed by:
Michael E. Böttcher,
Leibniz Institute for Baltic Sea Research (IOW), Germany
Weiqiang Li,
Nanjing University, China

****Correspondence:***
Dalton S. Hardisty
hardist1@msu.edu

Specialty section:
This article was submitted to Geochemistry, a section of the journal Frontiers in Earth Science

Received: *23 February 2021*
Accepted: *21 April 2021*
Published: *28 May 2021*

Citation:
Hardisty DS, Riedinger N, Planavsky NJ, Asael D, Bates SM and Lyons TW (2021) Holocene Spatiotemporal Redox Variations in the Southern Baltic Sea. Front. Earth Sci. 9:671401. doi: 10.3389/feart.2021.671401

INTRODUCTION

Bottom water oxygen availability in the Baltic Sea is regulated by a combination of warming temperature, eutrophication, salinity stratification, and controls related to basin morphology (Carstensen et al., 2014). Among these, increased nutrient input from land and associated cyanobacterial blooms are most prominently responsible for the tenfold increase in the seafloor area of Baltic low oxygen/anoxic bottom waters observed over the last century, while it has only been over the last 20 years that increased respiration resulting from anthropogenic warming is observable (Carstensen et al., 2014). Importantly, however, even in the absence of anthropogenic factors, salinity gradients and temporal variation from combined natural climate change, unique circulation patterns, and hydrography prime the Baltic Sea for the development of low oxygen bottom waters (Mohrholz et al., 2015). The Baltic Sea is silled at the Danish straits (**Figures 1A,B**), forcing freshwater output from runoff and saline input from the North Sea through the same location. This restriction supports the development of a strong halocline—limiting physical mixing between surface and bottom waters and thus limiting bottom water renewal to lateral advection. Such restricted and stratified conditions are particularly prone to the development of oxygen-depleted bottom waters (**Figures 1C–E** red lines), as is observed in other silled basins including the Black Sea, Cariaco Basin, Framvaren Fjord, and Saanich Inlet. Like these other restricted basins, the modern Baltic water column is reducing enough within some sub-basins to permit the accumulation of hydrogen sulfide—a water column redox state referred to as euxinia (Carstensen et al., 2014; Noordmann et al., 2014). Euxinia precludes the presence of animals and results in strong sequestration of a suite of redox-sensitive metals (for example, Mo and Fe) (Algeo and Lyons, 2006; Lyons and Severmann, 2006; Scott and Lyons, 2012).

The Baltic is unique relative to other modern anoxic settings such as the Black Sea, as the halocline is highly dynamic, with gradients in the spatial ranges, timescales, and depths of salinity fluctuation along transects moving away from the sill (**Figures 1C–E** blue lines). Baltic Sea salinity gradients and short-term oscillations are largely a function of isolated climatic events known as Major Baltic Inflows (MBIs). During these events, saline and oxygen-rich marine waters from the North Sea are introduced into the Baltic beneath the halocline (Carstensen et al., 2014). The MBIs are both barotropic and baroclinic events in which wind and air pressure cause a sea level difference between the Kattegat and Arkona Basin on opposing sides of the sill (**Figure 1**), forcing temporary net inflow of North Sea saline and oxygenated water into the Baltic (Franck et al., 1987; Matthäus, 2006; Mohrholz et al., 2015). Depending on the spatial scale of the MBI and the season of occurrence, most of Baltic Sea can become temporarily oxygenated. This extreme can lead to the oxidation of redox-sensitive chemical species accumulated in the formerly anoxic bottom waters (e.g., Mn(II), Fe(II), H_2S), while simultaneously introducing saline water that maintains the halocline and resulting stratification responsible for the return to and long-term maintenance of anoxic bottom waters (Huckriede and Meischner, 1996; Dellwig et al., 2010, 2018; Scholz et al., 2018; Hermans et al., 2019; Ni et al., 2020; van de Velde et al., 2020). Ultimately, halocline stability and frequency of bottom water renewal act to regulate the maximum reducing potential of bottom waters within individual Baltic sub-basins, resulting in an increased spatial gradient in the occurrence of euxinia and stable anoxic conditions more generally with increasing distance from the sill (**Figures 1C–E** red lines).

The Baltic Basin has undergone a complex evolution since the last glacial maximum, resulting in multiple transitions between freshwater and brackish and naturally occurring ancient anoxic events. Immediately following the last glacial maximum (∼22 ka), melting from the Scandinavian ice sheet formed an ice lake in the Baltic Basin, which eventually underwent a permanent switch to a brackish basin following global sea level rise and resulting connection to the open ocean—the Ancylus Lake-to-Littorina Sea transition—at approximately 8.5 ka (Andrén et al., 2011). Following this transition and associated halocline formation, two major pre-anthropogenic Baltic anoxic periods are known through sedimentary laminations and geochemical signatures (Manheim, 1961; Suess, 1979; Sohlenius, 1996; Sohlenius et al., 1996, 2001; Sternbeck and Sohlenius, 1997; Lepland and Stevens, 1998; Sohlenius and Westman, 1998; Zillén et al., 2008; Mort et al., 2010; Jilbert and Slomp, 2013; Jilbert et al., 2015; Lenz et al., 2015b; Hardisty et al., 2016; Dijkstra et al., 2018a,b; Groeneveld et al., 2018; van Helmond et al., 2018). These events roughly overlap with the Holocene Thermal Maximum (HTM) (8–4 ka) and Medieval Climate Anomaly (MCA) (1.2–0.8 ka) and co-occur with the widespread enhanced deposition of organic matter in many sub-basins (Zillén et al., 2008).

Recent studies of paleoredox conditions for individual sub-basins during these intervals stress that, like today, specific paleoredox regimes have differed among the sub-basins during penecontemporaneous low oxygen events. Further, paleoredox regimes differed among temporally distinct anoxic events within the same sub-basin. For instance, in the currently well-oxygenated Bothnian Sea, paleoredox records provide evidence for relatively stable euxinia during the HTM, while indicating well-oxygenated water column conditions during the MCA (Jilbert et al., 2015; Dijkstra et al., 2018b). In the Landsort Deep, a currently semi-permanently euxinic basin, paleoredox records provide evidence for euxinic conditions during the MCA and HTM (Dijkstra et al., 2016; Hardisty et al., 2016). Paleo-proxy data specific to well-defined paleoredox regimes and anoxic timescales relevant to the modern redox states are relatively sparse from southern Baltic sub-basins, which elevates the importance of this study.

The redox conditions of modern and ancient basins can be quantified by determining the accumulation of reduced products indicative of the main metabolic processes within a specific zone (e.g., Mn, Fe, or S reduction) (Froelich et al., 1979; Canfield and Thamdrup, 2009). Here, we apply Mo, Mn, Fe, and S geochemistry to define the degree to which reduced Mn (manganous) versus Fe (ferruginous) versus S (euxinic) acted as primary redox buffers in the water column—a sequence representing progressively more reducing conditions. We specifically focus on the ancient water columns of southern Baltic sub-basins Lille Belt, Bornholm Basin, and Landsort Deep.

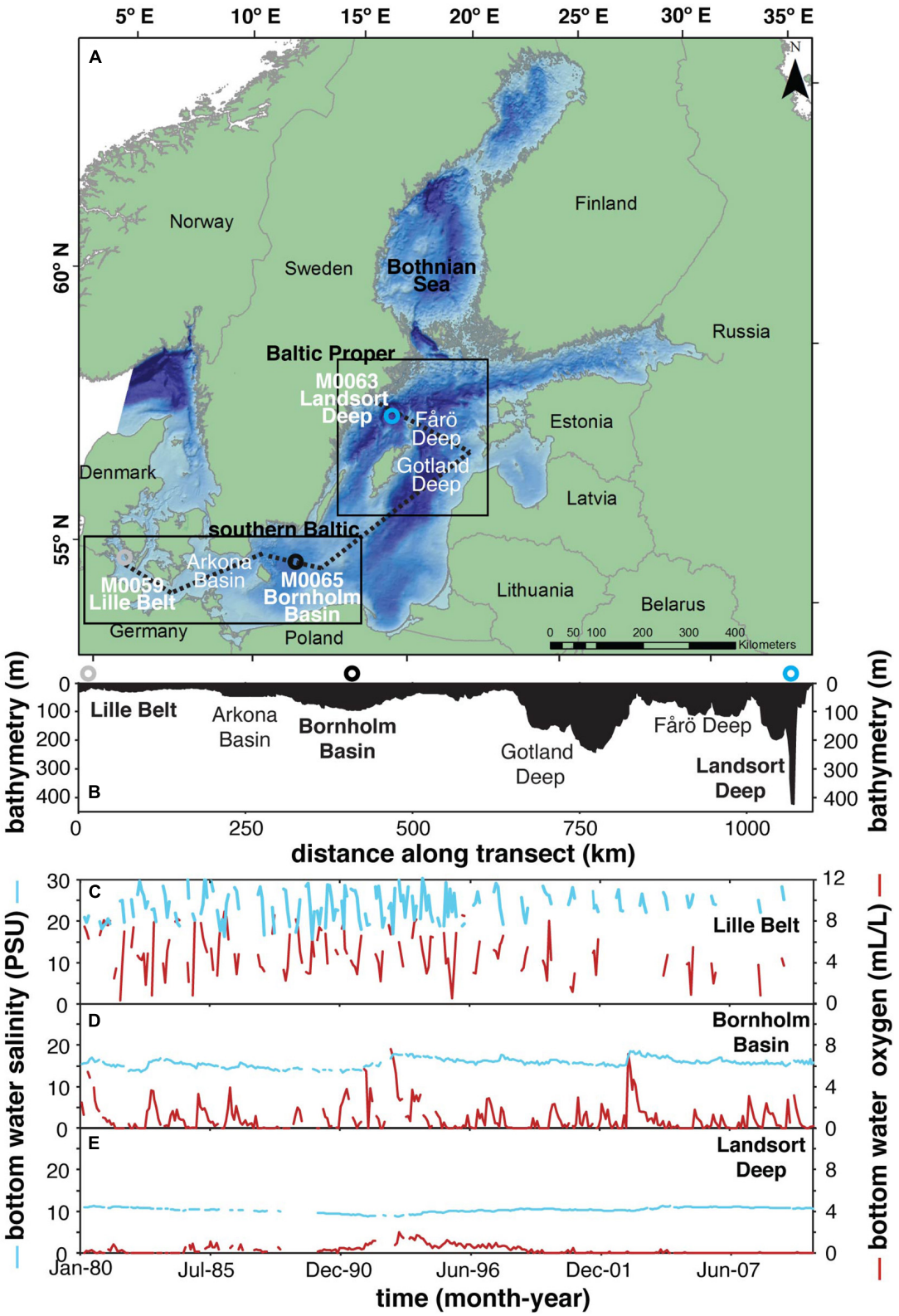

FIGURE 1 | (A) Map showing relevant drilling localities from IODP Expedition 347 and other locations discussed in the text. **(B)** Bathymetry from transect shown in panel **(A)** (dashed line). Panels **(C–E)** represent the mean monthly (1980–2010) bottom water salinity and oxygen concentrations at Lille Belt, Bornholm Basin, Landsort Deep, respectively, from the Baltic Environmental Database of the Baltic Nest Institute, Stockholm University, specifically from stations 450, BY5, and BY31. The red and blue lines represent dissolved oxygen and salinity, respectively.

These sub-basins form a sill-proximal to sill-distal transect (**Figure 1**). We use cores from Integrated Ocean Drilling Program (IODP) Expedition 347 and combined sedimentology; trace element concentrations and Fe speciation; Mo, S, and Fe isotopes; and pore water geochemistry to constrain the specific paleoredox regimes. Our records are combined with previously published data from the Baltic and Bothnian Seas to reconstruct spatiotemporal redox conditions across the Baltic Holocene.

BACKGROUND

Paleoredox Proxy Geochemistry

Ratios of total Fe-to-aluminum (Fe_T/Al) and "highly reactive" Fe-to-total Fe (Fe_{HR}/Fe_T) are related proxies for determining paleo-water column redox, highlighting oxic, ferruginous (Fe-rich), and euxinic conditions (Raiswell et al., 2018). "Highly reactive" Fe represents operationally defined Fe-bearing minerals that are reactive toward hydrogen sulfide on short diagenetic timescales to form Fe sulfides, as well as any Fe sulfides that have formed (Canfield and Berner, 1987; Canfield, 1989; Canfield et al., 1992, 1996; Raiswell and Canfield, 1998; Poulton and Canfield, 2005). Comparisons of Fe_T/Al and Fe_{HR}/Fe_T ratios among sediments from the stable euxinic Black Sea and other similar settings relative to oxic continental margin and deep ocean sediments indicate that "highly reactive" Fe is enriched relative to typical detrital fluxes under anoxic conditions through a process coined the "Fe shuttle" (Canfield et al., 1996; Raiswell and Canfield, 1998; Lyons et al., 2003; Lyons and Severmann, 2006). Detrital values for Fe_{HR}/Fe_T are typically <0.38 in oxic settings (Raiswell and Canfield, 1998). The detrital Fe_T/Al in the Baltic has been specifically calibrated as <0.65 (Fehr et al., 2008). Values clearly above these thresholds represent paleo-anoxic water columns. Pyrite-to-"highly reactive" ratios (Fe_{py}/Fe_{HR}) greater than ∼0.7 in settings with independent indications of anoxia indicate that the majority of the "highly reactive" Fe has formed pyrite, which often results from syngenetic pyrite formation in the water column under euxinic conditions (Canfield et al., 1996; Lyons, 1997; Wijsman et al., 2001b; Lyons and Severmann, 2006; Poulton and Canfield, 2011). Importantly, when Fe_T/Al and Fe_{HR}/Fe_T are not enriched, ratios of Fe_{py}/Fe_{HR} are a proxy for sulfide accumulation in ancient pore waters (Sperling et al., 2015; Hardisty et al., 2018).

Molybdenum cycling can be applied to fingerprint ancient euxinic conditions—but also Fe and Mn cycling. Molybdate is the dominant dissolved Mo species in oxic seawater and is largely sourced from rivers, with a typical concentration near 104 nM in normal oxic marine waters (Miller et al., 2011; Neubert et al., 2011), but with values near ∼20 nM in the brackish Baltic Sea (Noordmann et al., 2014). The largest Mo sink in modern seawater is sorption to Mn and Fe oxides, which deliver molybdate to the sediments until burial and dissolution of the oxides during anoxic diagenesis (Bertine and Turekian, 1973; Krishnaswami, 1976; Kashiwabara et al., 2009). If sulfide is present at appreciable levels, molybdate will convert to tetrathiomolybdate and other polysulfide species (Erickson and Helz, 2000; Dahl et al., 2013; Azrieli-Tal et al., 2014), which are efficiently buried in association with organic matter and sulfides (Erickson and Helz, 2000; Algeo and Lyons, 2006; Dahl et al., 2013, 2017; Azrieli-Tal et al., 2014; Wagner et al., 2017; Vorlicek et al., 2018; Ardakani et al., 2020). This process is favored by relatively high levels of dissolved sulfide. Sediments underlying euxinic waters have elevated Mo concentrations, typically >25 ppm if not much larger (Scott and Lyons, 2012). Lower sedimentary Mo concentrations, but elevated relative to average continental crust of <2 ppm can occur under conditions where sulfide accumulates in pore waters (Taylor and McLennan, 1995; Neubert et al., 2008; Nägler et al., 2011; Scott and Lyons, 2012; Hardisty et al., 2018). Muted enrichments are also a signature of elevated sedimentation rates even under euxinic conditions (Lyons and Kashgarian, 2005; Morford et al., 2009; Hardisty et al., 2018) and in restricted euxinic basins where the sedimentary Mo removal flux outpaces the marine supply (Algeo and Lyons, 2006).

The modern Gotland and Landsort Deep water columns have Mo isotope values of 2.22–2.49‰ (Noordmann et al., 2014), which is similar to that of open ocean seawater (∼2.3‰; Siebert et al., 2003). In stable and restricted euxinic settings with total sulfide concentrations beyond ∼100 μM (e.g., the Black Sea) near-quantitative scavenging of water column Mo in the presence of this ample free sulfide results in sedimentary Mo isotope signatures that mirror that of seawater (Barling et al., 2001; Siebert et al., 2003; Arnold et al., 2004; Neubert et al., 2008; Nägler et al., 2011; Noordmann et al., 2014). Under conditions with unstable euxinia and/or total sulfide concentrations <100 μM, such as the modern Landsort and Gotland Deeps, Mo concentrations are often still elevated relative to oxic settings, but a negative Mo isotope fractionation linked to incomplete conversion of molybdate to tetrathiomolybdate of up to ∼3‰ is captured in the sediments (Tossell, 2005; Neubert et al., 2008; Nägler et al., 2011; Azrieli-Tal et al., 2014; Noordmann et al., 2014). Importantly, however, sorption of Mo to Mn and Fe oxides also exerts negative Mo isotope fractionation relative to seawater as large as 2.9‰ (Barling et al., 2001; Wasylenki et al., 2008) and 2.2‰ (Goldberg et al., 2009), respectively. Smaller negative Mo isotope fractionations near −1.0‰ have also been demonstrated during assimilation and adsorption to organic matter (Zerkle et al., 2011; Kowalski et al., 2013).

MATERIALS AND METHODS

Sample Collection

Coring details, sedimentological, and paleontological descriptions for each site have been summarized previously (Andrén et al., 2015a,b,c). Samples from M0059C,E and M0065C (locations and water depth shown in **Figure 1**) were collected and sealed in N_2-flushed bags onboard the ship immediately following core recovery and stored frozen prior to analysis—minimizing oxidation of redox sensitive Fe minerals important for this study. Cores from M0059A,B,D and M0065A,B were capped and sealed immediately following retrieval and stored at 4°C prior to sample collection, which occurred 4–5 months later at MARUM in Bremen, Germany. Sediments were analyzed at

the University of California, Riverside and Yale University. As described below, we used exclusively fresh material for analysis, scraping and discarding any oxidized sediments.

At M0065, due to potential mustard gas contamination, the upper 2 m of the sediments were not collected and hence the cores from the Bornholm Basin do not clearly capture the MCA. In the absence of age constraints, the broad peak and associated sub-peaks in total organic carbon (TOC) at this site are interpreted to reflect the HTM.

Geochemical Methods

Lille Belt and Bornholm Basin Sediments

Splits of freshly thawed sample were used for the sequential extraction of iron monosulfide phases or acid volatile sulfide (AVS) (mainly iron monosulfides, FeS) (Berner et al., 1979; Chanton and Martens, 1985; Morse and Cornwell, 1987; Lyons, 1997; Hurtgen et al., 1999) and chromium reducible sulfur (CRS) (mainly pyrite, FeS_2) (Canfield and Berner, 1987). The CRS and AVS concentrations were measured via the methylene blue method using a spectrophotometer at wavelength of 660 nm (Cline, 1969). The AVS and CRS fractions were not determined in sequence, thus the pyritic sulfur was determined by subtracting the AVS from CRS, which was then used to calculate the associated Fe concentrations (Fe_{AVS} and Fe_{py}) using the stoichiometries FeS and FeS_2, respectively.

A modified chemical extraction method was applied for characterization of distinctive operationally defined "highly reactive" Fe pools: ascorbate (Fe_{asc}), dithionite (Fe_{dith}), oxalate (Fe_{ox}), and Na-acetate (Fe_{NaAc})—representing labile Fe-oxides, crystalline Fe-oxides, magnetite, and Fe-carbonate, respectively (Kostka and Luther, 1994; Raiswell et al., 1994, 2010; Poulton and Canfield, 2005). Using the same procedure as Hardisty et al. (2016), care was taken during the extractions to prevent artificial inflation of Fe-oxide phases via oxidation of Fe-sulfides or modifications associated with powdering (Raiswell et al., 1994, 2010). Specifically, (1) samples were collected, sealed in bags with N_2 headspace, and immediately frozen onboard IODP 347; (2) only fresh and frozen samples were used for the Fe extractions; (2) samples were not powdered; (3) sample exposure time to the atmosphere was limited to minutes during initial weighing and subsequent reagent additions; (4) all chemical reagents were deoxygenated with N_2 for at least 15 min prior to addition to the sample; (5) the headspace of each centrifuge tube was replaced with N_2 prior to shaking during the extractions. All Fe extracts were quantified via an Agilent 7500ce quadrupole inductively coupled plasma-mass spectrometer (ICP-MS) at UC Riverside following dilution with 0.3 M nitric acid. Separate sub-sample duplicates and triplicates assessed for precision revealed relative whole analysis standard deviations in most cases <0.01 weight % but in a few cases <0.05 weight %; we point out, however, that heterogeneities are expected, as bulk samples were not homogenized prior to taking a sub-sample for the sequential Fe-extraction procedure.

Total carbon and total inorganic carbon (TIC) were determined using an Eltra CS-500 carbon-sulfur analyzer at UC Riverside. TOC was calculated by subtracting TIC from total carbon. The standard reference material (SRM) AR4007 was analyzed routinely, with values within the reported range of 7.32 ± 0.12 wt. %.

Trace metal contents of bulk sediment were determined through a multi-acid digest procedure using dried samples which were powdered and ashed at 450°C for site M0065 and 650°C for site M0059 samples and then digested using trace metal grade HF, HNO_3, and HCl acids, with the residue solubilized as the final step in 0.3 M nitric acid. The ashing temperature was increased for site M0059 samples due to an insoluble residue only observed when ashed at lower temperatures. Each batch of total digests included an SRM for quality control. Total digests were measured for major elements and trace elements via an Agilent 7900 quadrupole ICP-MS at UC Riverside using a multi-element standard solution in a 0.3 M nitric acid matrix. SRMs NIST 2702, USGS SCO-1, and USGS SGR-1 were digested and analyzed in parallel with each batch of samples with all elements analyzed falling within reported ranges.

Molybdenum isotope measurements were performed at the Metal Geochemistry Center at Yale University, New Haven, Connecticut, using the Neptune Thermo Scientific multicollector ICP-MS (Asael et al., 2013, 2018). The 0.3 M nitric acid total digest solution was evaporated and re-constituted in 7 M HCl. An aliquot of the acid split was spiked with a ^{97}Mo–^{100}Mo double spike solution—prepared gravimetrically from Oak Ridge Laboratory metal powders as previously described (Asael et al., 2013, 2018)—according to the Mo concentration determined previously via ICP-MS in order to maintain a constant sample-to-spike ratio. This aliquot was also used for chromatographic separation. A two-stage column procedure was applied for Mo purification: the sample was run through an anion resin (AG-MP-1M) to separate Mo and Fe from the matrix followed by purification through a cation resin (AG50W-X8) to separate Mo from any remaining Fe. Molybdenum isotope compositions are reported using the δ notation, where:

$$\delta^{98}\mathrm{Mo} = \left[\left(^{98}\mathrm{Mo}/^{95}\mathrm{Mo}\right)_{\mathrm{sample}} \Big/ \left(\left(^{98}\mathrm{Mo}/^{95}\mathrm{Mo}\right)_{\mathrm{NIST}} \times 0.99975\right) - 1\right] \times 1000, \quad (1)$$

where $\delta^{98}Mo$ is calculated relative to NIST 3134 (Lot 130418) with a value of −0.25‰ (Nägler et al., 2014). A calibration of the NIST standard relative to Rochester (Lot 862309E) gave:

$$\delta^{98}\mathrm{Mo}_{\mathrm{ROCH}} = \delta^{98}\mathrm{Mo}_{\mathrm{NIST3137}} - 0.32 \pm 0.12‰, \quad (2)$$

Duplicates (n = 6) of reference standard NOD-1 yielded an average $\delta^{98}Mo$ value of −0.63‰ and 1σ of 0.18‰, similar to previously reported values (Asael et al., 2013). Values for Mo isotope measurements and associated error can be found in **Supplementary Tables 1, 2**. Measured errors for individual samples were <0.07‰ but largely <0.04‰.

Landsort Deep Sediments

The Fe extractions, elemental abundances, and Mo isotope compositions from Landsort Deep were previously characterized and reported in Hardisty et al. (2016) according to the same methods described above for Lille Belt and Bornholm Basin. For the current study, we used splits from specific eluents from the Mo isotope chromatographic separation procedure in Hardisty et al. (2016) to measure the Fe isotope composition of bulk sediments. These procedures are described below. In the current study, we also used the TRS and AVS fractions from Hardisty et al. (2016) to determine and report the S isotope composition of reduced sulfides.

Iron isotopes were analyzed for Landsort Deep bulk sediments at the Metal Geochemistry Center at Yale University using the Neptune Thermo Scientific multicollector ICP-MS. Total digests and chromatographic separation for the measurement of Mo isotopes (but not Fe isotopes) were already performed for Hardisty et al. (2016) according to the same procedures described in section "Lille Belt and Bornholm Basin Sediments" for Bornholm Basin and Lille Belt sediments. For the present study, we diluted the Fe fraction—separated during the Mo purification procedure with AG-MP-1M resin during Hardisty et al. (2016)—for measurement of Fe isotopes. Corrections for instrumental mass discrimination were performed using conventional sample-standard bracketing (Busigny et al., 2014), and $^{56}Fe/^{54}Fe$ ratios are expressed in the standard delta notation in per mil (‰) relative to IRMM-014 (Taylor et al., 1992):

$$\delta^{56}\mathrm{Fe} = \left[\left(^{56}\mathrm{Fe}/^{54}\mathrm{Fe}\right)_{\mathrm{sample}} \Big/ \left(^{56}\mathrm{Fe}/^{54}\mathrm{Fe}\right)_{\mathrm{standard}} - 1 \right] \times 1000, \quad (3)$$

We processed a $FeCl_2$ standard alongside the samples, which has a reported value of -0.71 ± 0.18‰ (Teutsch et al., 2009), and report a mean value -0.62 ± 0.12‰ (2SD), which overlaps within error.

Sulfur isotopes of total reduced S (TRS) and AVS fractions from Landsort Deep were measured at the University of California Riverside. TRS and AVS concentrations, but not S isotope compositions, were reported in Hardisty et al. (2016) using the same technique of converting to ZnS described in section "Lille Belt and Bornholm Basin Sediments" for sediments at Lille Belt and Bornholm Basin. For the current study, we used a chromium reduction to convert the ZnS from both AVS and TRS [used for concentration determinations in Hardisty et al. (2016)] to Ag_2S using the same technique described in section "Lille Belt and Bornholm Basin Sediments" for CRS but by replacing the ZnAc trap with $AgNO_3$. The Ag_2S precipitates were then filtered, dried, and homogenized before weighing into tin capsules with excess V_2O_5. The $^{34}S/^{32}S$ ratio for samples were measured using a Thermo Delta V gas-source isotope-ratio mass spectrometer coupled to a Costech 4010 elemental combustion system via a ConFlo III interface for on-line sample combustion and analysis. All sulfur isotope compositions are reported in standard delta notation as permil (‰) deviation relative to Vienna Canyon Diablo Troilite and were corrected using replicate analyses of International Atomic Energy Agency (IAEA) standards IAEA-S1 (−0.3‰), IAEA-S2 (+22.65‰), and IAEA-S3 (−32.5‰). Corrected values for IAEA standards are all within reported ranges with IAEA-S1 of -0.3 ± 0.47‰ ($n = 16$), IAEA-S2 of $+22.7 \pm 0.47$‰ ($n = 15$), and IAEA-S3 of -32.45 ± 0.33‰ ($n = 15$). A total of 21 samples were analyzed in duplicate or replicate for TRS and AVS, with the majority having standard deviations <1.0‰; however, a few samples, particularly those from the upper sapropel, had significantly larger standard deviations. Given the robust observations between replicates generally and the IAEA standards, we recommend that these variations reflect real heterogeneities, as samples for AVS, TRS, and Fe speciation were drawn directly from wet sediment that was not pre-homogenized in order to limit pyrite and AVS oxidation (Hardisty et al., 2016).

RESULTS

At Lille Belt (**Figure 2**), TOC is <1 wt. % from the bottom of the core up to ∼52 mcd, where TOC increases to 3.75 wt. % and gradually increases up the remainder of the core (**Figure 2B**). Superimposed on this increasing TOC trend are two sapropel units at 51.2–44.6 and 7.7–5.9 mcd, with peak values of ∼6.2 and 7.8 wt. %, respectively. Manganese concentrations show a broad peak from 47.5 to 11 mcd, with values oscillating but peaking as high as 1.5 wt. % (**Figure 3C**). "Highly reactive" Fe is reported as the sum of Fe_{AVS}, Fe_{py}, Fe_{asc}, Fe_{dith}, Fe_{ox}, and Fe_{NaAc}. Because of the presence of significant Fe_{AVS} at Lille Belt, we amend the typically reported Fe_{py}/Fe_{HR} to include Fe_{AVS}, thus $(Fe_{py}+Fe_{AVS})/Fe_{HR}$. The Fe_T/Al ratios generally fall around the Baltic detrital baseline of 0.65, and Fe_{HR}/Fe_T ratios are near established thresholds for anoxic conditions but are generally <0.5 (**Figures 3D,E**). The $(Fe_{py}+Fe_{AVS})/Fe_{HR}$ values oscillate but remain <0.7 (**Figure 3F**). The Mo contents are <25 ppm, with the exception of one sample with a concentration of 30.9 ppm (**Figure 3G**). Molybdenum isotope values are between +0.18 to +1.47‰ throughout the sediment column (**Figure 3H**). We note that trends and values in Mo concentration and Fe speciation are similar to those of a previous study of the same core that evaluated a separate sample set (van Helmond et al., 2017). All Lille Belt data are available in **Supplementary Table 1**.

At Bornholm Basin (**Figure 3**), TOC values are below 0.7 wt. % from the bottom of the profile up to 12.75 mcd followed by a steady increase up core throughout the remaining sediment column (**Figure 3B**). There are two peaks between 12.3 and 8.3 mcd and 5.17 and 3.34 mcd to values of ∼4.2 and 6.6 wt. %, respectively. At Bornholm Basin, multiple anoxic indicators fluctuate in association with the two sapropels with elevated TOC (**Figure 4**). Manganese concentrations increase up core exclusively from 9.8 to 6.6 mcd (**Figure 3C**). The Fe_T/Al ratios are generally at or below a baseline of <0.65 other than within the two intervals where TOC peaks (**Figure 3D**). Within these upper and lower sapropels, the Fe_T/Al values increase to 0.69 and 0.90, respectively. Other than within the sapropels, the Fe_{HR}/Fe_T ratio generally stays below 0.38 (**Figure 3E**). Fe_{AVS} was not found to be a significant component (<0.01 wt. %) at Bornholm Basin and was not measured for all samples, but we still maintain the $(Fe_{py}+Fe_{AVS})/Fe_{HR}$ nomenclature

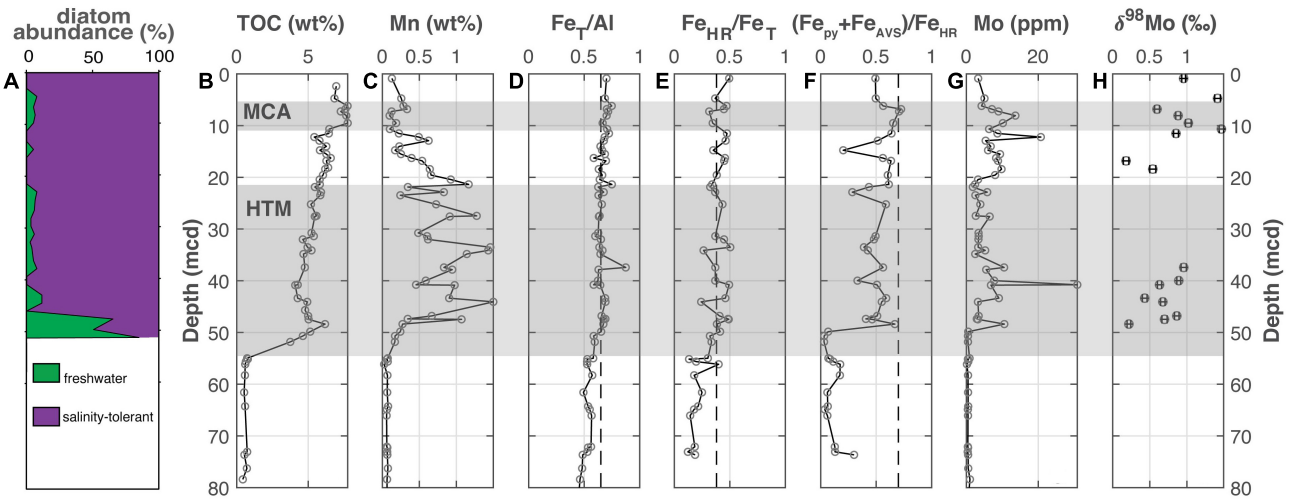

FIGURE 2 | Lille Belt (M0059). **(A)** The abundance of freshwater versus salinity tolerant diatoms [Andrén et al., 2015a; also see Kotthoff et al. (2017) and Warnock et al. (2020) for more detailed reconstructions], **(B)** total organic carbon, **(C)** manganese, **(D)** iron-to-aluminum, **(E,F)** Fe speciation, **(G)** molybdenum concentrations, and **(H)** molybdenum isotopes. The Medieval Climate Anomaly and Holocene Thermal Maximum are highlighted with the horizontal gray bars based on the geochronology from van Helmond et al. (2017) for M0059. Vertical dashed lines for Fe_T/Al, Fe_{HR}/Fe_T, and $(Fe_{py}+Fe_{AVS})/Fe_{HR}$ note thresholds for anoxia, euxinic and ferruginous conditions discussed in the main text.

for simplicity when comparing between the other cores. The Fe_{HR}/Fe_T values increase to 0.62 and 0.43 in the lower and upper sapropel, respectively. Notably, there is a muted Fe_{HR}/Fe_T peak up to 0.43 at 8.1 mcd that is outside of the two main increases in TOC but that overlaps with distinct minima in each $(Fe_{py}+Fe_{AVS})/Fe_{HR}$ and Mo concentration and the main peak in Mn concentrations. Values for $(Fe_{py}+Fe_{AVS})/Fe_{HR}$ are below 0.2 from the bottom of the profile to 10.3 mcd, where values begin to increase to >0.7 for most of the overlying sequence (**Figure 3F**). Molybdenum concentrations are generally <2 ppm from the bottom of the profile to near 9.8 mcd (**Figure 3G**). Above 9.8 mcd, Mo concentrations increase but stay below 27 ppm. Molybdenum isotope values range from −0.29 to +1.04‰ but are distinctly more positive from 6.54 to 3.85 mcd (**Figure 3H**). All Bornholm Basin data are available in **Supplementary Table 2**.

A previously published study from the Landsort Deep includes the Fe speciation and Mo concentration and isotope data shown in **Figures 4A–H** (Hardisty et al., 2016), which are included here for comparison to data discussed in sections "Lille Belt Paleoredox" and "Bornholm Basin Paleoredox" for the southern Baltic sub-basins. The new Fe and S isotope data are shown in **Figures 4I,J**. Iron isotope data from bulk sediments range from −0.12 to +0.46‰ and show distinct negative excursions within the sapropel units, along with corresponding increases in Fe_T/Al, Fe_{HR}/Fe_T, and $(Fe_{py}+Fe_{AVS})/Fe_{HR}$ and other redox-sensitive indicators. The S isotope data from TRS and AVS fractions are displayed together in **Figure 4I** and show overlapping trends. All new Fe and S isotope data from Landsort Deep are available in **Supplementary Tables 3, 4**, respectively.

The pore water dissolved Fe profiles are shown from Lille Belt, Bornholm Basin, and Landsort Deep in **Figure 5**. These data are also reported in the IODP Expedition 347 Reports (Andrén et al., 2015a,b,c) and used as part of detailed diagenetic models in Egger et al. (2017) and Dijkstra et al. (2018a).

DISCUSSION

Our data reveal multiple geochemical transitions in each core consistent with spatiotemporal redox variations associated with increases in organic carbon content. The previous studies discussed and cited in the next section have noted similar changes in organic carbon content at these sites and even in the same IODP cores. In combination with changes in diatom assemblages and other proxies, these past studies provide some context for the relative timing of each of these transitions and hence a more comprehensive reconstruction of spatiotemporal redox variations in the Baltic Sea. These previous studies are discussed below as context for our new results.

Salinity Transitions and Correlations Between Sub-Basins

The combination of carbon and diatom records from this and past studies indicates periods of variable salinity and organic matter preservation, which were already well known from the Baltic. These intervals and horizons are markers that can be used to correlate syndepositional periods and events among the sub-basins. The Lille Belt, Bornholm Basin, and Landsort Deep show a systematic shift in diatom assemblage marking the transition from lacustrine to brackish/marine water column conditions—that is, the Ancylus Lake to Littorina Sea transition (**Figures 2A**, **3A**, **4A**; Sohlenius et al., 2001; van Wirdum et al., 2019; Warnock et al., 2020). The Initial Littorina Stage, the transition period between the lacustrine Ancylus Lake and brackish Littorina Sea, lasted from ∼9.8 to 8.5 ka and is

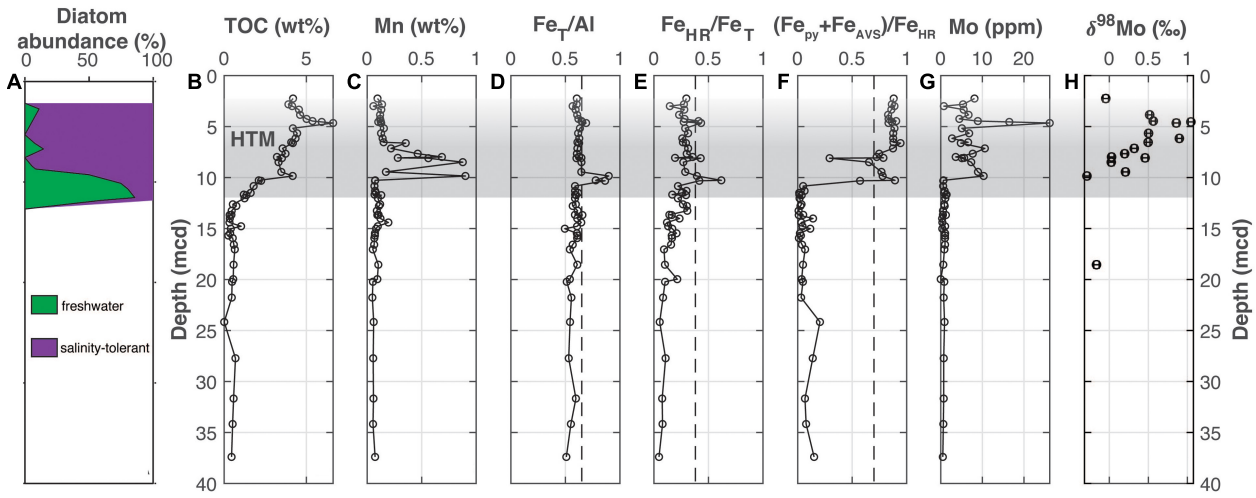

FIGURE 3 | Bornholm Basin (M0065). **(A)** The abundance of freshwater versus salinity tolerant diatoms (Andrén et al., 2015b), **(B)** total organic carbon, **(C)** manganese, **(D)** iron-to-aluminum, **(E,F)** Fe speciation, **(G)** molybdenum concentrations, and **(H)** molybdenum isotopes. The Medieval Climate Anomaly and Holocene Thermal Maximum is highlighted with the horizontal gray bar but is shaded upward to highlight uncertainty in locating the end of the HTM due to a lack of chronological constraints. Vertical dashed lines for Fe_T/Al, Fe_{HR}/Fe_T, and $(Fe_{py}+Fe_{AVS})/Fe_{HR}$ note thresholds for anoxia, euxinic and ferruginous conditions discussed in the main text. Note that the axis label in part F includes Fe_{AVS} in the numerator for simplicity and uniformity when comparing results between sites in the text, but that—as discussed in the results—Fe_{AVS} was negligible in a sample survey from site M0065 and was therefore was not measured in all samples.

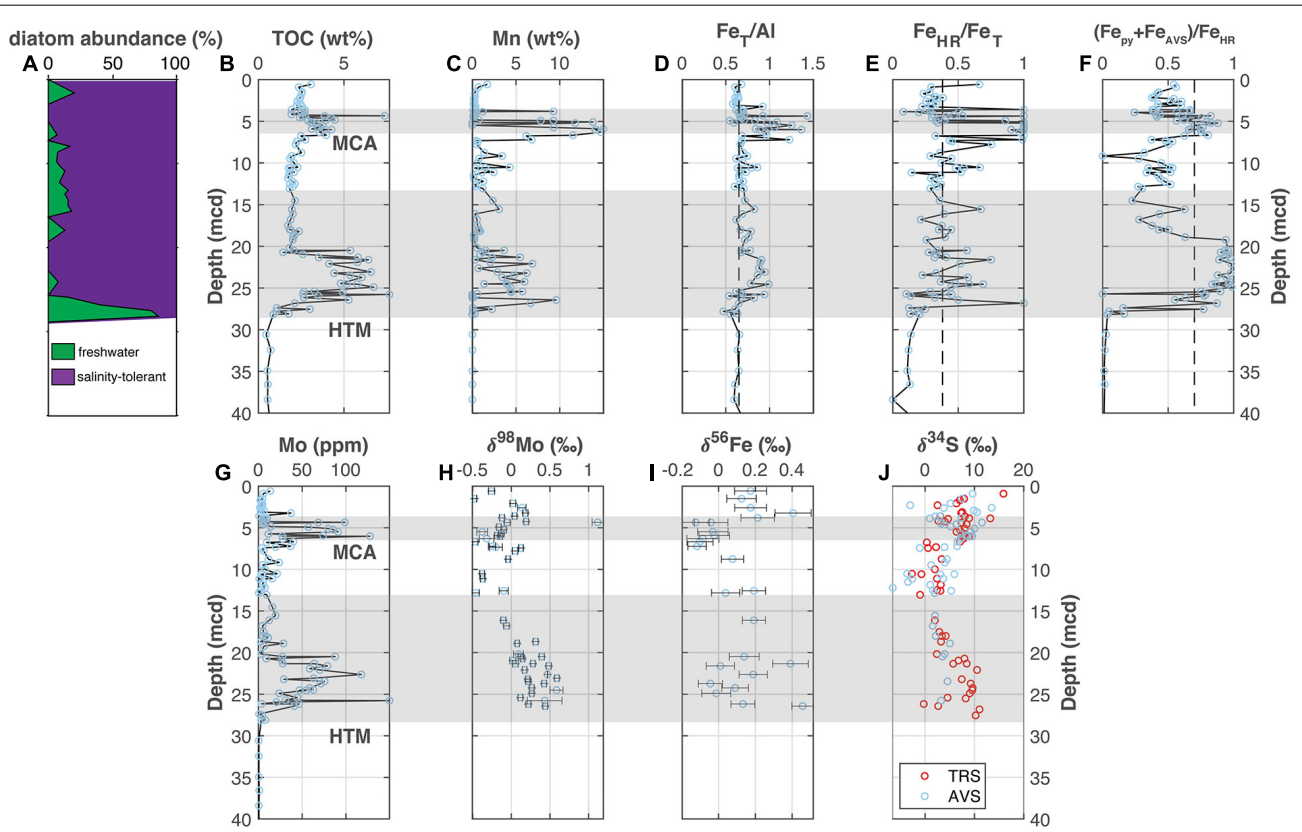

FIGURE 4 | Landsort Deep (M0063). **(A)** The abundance of freshwater versus salinity tolerant diatoms [Andrén et al., 2015c; also see van Wirdum et al. (2019) for more detailed reconstructions], **(B)** total organic carbon, **(C)** manganese, **(D)** iron-to-aluminum, **(E,F)** Fe speciation, **(G)** molybdenum concentrations, **(H)** molybdenum isotopes, **(I)** iron isotopes, and **(J)** sulfur isotopes. The Medieval Climate Anomaly and Holocene Thermal Maximum are highlighted with the horizontal gray bars based on the geochronology from van Wirdum et al. (2019) for M0063. Vertical dashed lines for Fe_T/Al, Fe_{HR}/Fe_T, and $(Fe_{py} + Fe_{AVS})/Fe_{HR}$ note thresholds for anoxia, euxinic and ferruginous conditions discussed in the main text. Geochemical data other than Fe and S isotopes come from Hardisty et al. (2016).

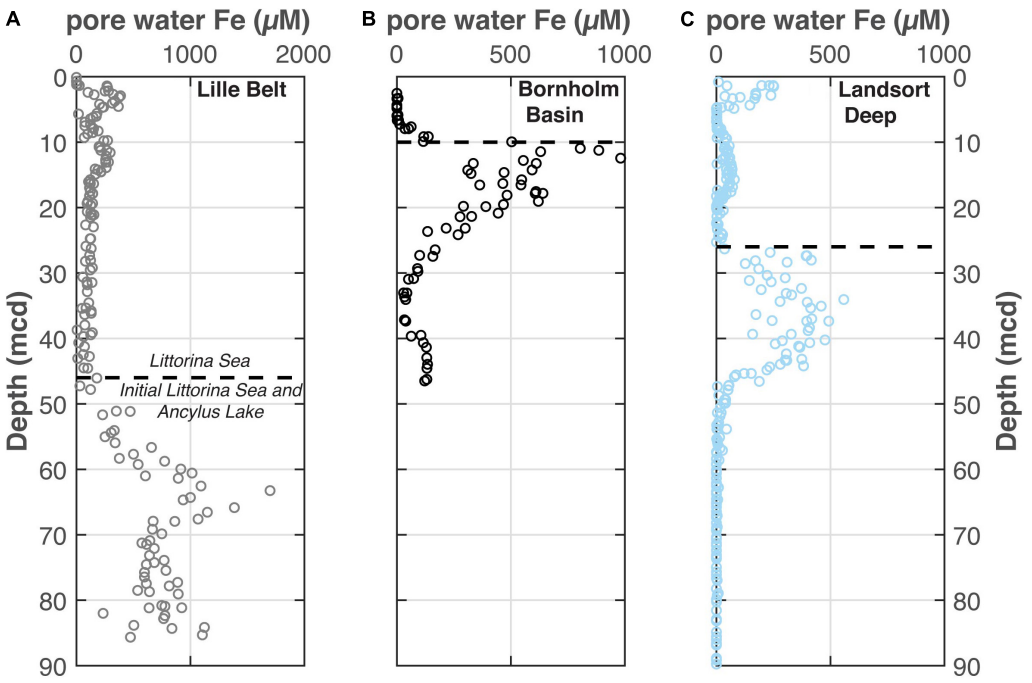

FIGURE 5 | The pore water Fe concentrations from each **(A)** Lille Belt, **(B)** Bornholm Basin, and **(C)** Landsort Deep. Data come from the IODP 347 Expedition Report (Andrén et al., 2015a,b,c; Egger et al., 2017). The dashed line from each site marks the horizon in the profile with the first indications of pore water sulfide accumulation, as constrained from Mo concentrations and $(Fe_{py}+Fe_{AVS})/Fe_{HR}$. In each case this occurs near the transition from the Ancylus Lake (AL) to the Littorina Sea (LS) noted from salinity-tolerant diatoms. Note the variations in the scale of the *x*-axis between these figures.

characterized by pulses of saline waters input into the Baltic Basin (Sohlenius et al., 2001; Björck et al., 2008; Andrén et al., 2011). The shift to sedimentary Mo concentrations >2 ppm (detrital values) alongside the increases in $(Fe_{py}+Fe_{AVS})/Fe_{HR}$ at each site at this transition in phase with the increases in TOC reflects accumulation of sulfide in the pore water (**Figures 2F,G**, **3F,G**, **4F,G**). Sulfide build up, in turn, was related to input of saline water and associated sulfate into the basin during the Initial Littorina Sea. The overlying interval where salinity-tolerant diatoms become relatively more abundant marks the onset of the Littorina Sea and the brackish conditions that still exist today (Sohlenius et al., 2001; van Wirdum et al., 2019; Warnock et al., 2020). This transition occurred 7500-7150 BP at Lille Belt (Kotthoff et al., 2017; Warnock et al., 2020).

Notably, there are peaks in TOC observed in each of the three cores. The lowermost peak can be linked to the HTM (**Figures 2B**, **3B**, **4B**), lasting from 8 to 4 ka (Jilbert and Slomp, 2013; Dijkstra et al., 2016; Hardisty et al., 2016; van Helmond et al., 2017). The HTM was marked by relatively higher temperatures and higher sea level and reduced freshwater input relative to today, likely representing the most saline period in the Baltic Sea since the LGM (Gustafsson and Westman, 2002; van Wirdum et al., 2019; Ni et al., 2020; Warnock et al., 2020). These factors likely contributed to the onset of anoxia observed during this interval (Papadomanolaki et al., 2018). Importantly, the HTM in the Bothnian Sea has been linked to more restricted conditions and widespread euxinia leading to the drawdown of Mo from the water column (Jilbert et al., 2015; Dijkstra et al., 2018b) thus, our Mo isotope data can be used to assess the potential of a syndepositional phenomenon in the southern Baltic sub-basins.

A secondary peak in TOC observed at Lille Belt (**Figure 2B**) and Landsort Deep (**Figure 4B**; Dijkstra et al., 2016, 2018a; Hardisty et al., 2016) is contemporaneous with the MCA (1.2–0.8 ka) and has been observed previously in both Fårö and Gotland Deeps (Jilbert and Slomp, 2013). Enhanced productivity and organic carbon burial during this interval occurred with warmer sea surface temperatures (Kabel et al., 2012; van Wirdum et al., 2019), all of which likely contributed to de-oxygenation during the MCA (Papadomanolaki et al., 2018).

Lille Belt Paleoredox

Individually, the paleoredox proxies at Lille Belt are not particularly diagnostic but together provide support for at least episodically manganous/ferruginous conditions with sulfide likely limited to the pore fluids. For example, intermittent laminations are observed, which are consistent with low oxygen conditions that persisted at least seasonally and largely excluded benthic fauna (Andrén et al., 2015a), a condition similar to that observed today (**Figure 1**). It is possible that low oxygen conditions excluded infaunal habitation outside of the laminated regions, but either seasonal or episodic returns to oxygenated conditions (e.g., MBIs) permitted burrowing and overprinting of laminations in these zones.

Geochemical evidence for at least intermittent anoxia comes from Fe_T/Al and Fe_{HR}/Fe_T values near or at thresholds associated

with anoxia. We note that elevated Fe_T/Al and Fe_{HR}/Fe_T ratios are a robust indicator of anoxic water columns supporting dissolved iron or hydrogen sulfide accumulation. Low water column oxygen levels but lacking sulfide and/or elevated dissolved Fe have not been shown to support increases in Fe proxy values (Hardisty et al., 2018). Our $(Fe_{py}+Fe_{AVS})/Fe_{HR}$ ratios are below the threshold interpreted for euxinia (Raiswell and Canfield, 1998), suggesting ferruginous conditions. Indeed, the persistence of significant non-subsidized "highly reactive" Fe, relatively high Fe_{AVS} (indicating incomplete conversion to pyrite; Berner et al., 1979; Hurtgen et al., 1999), and elevated pore water Fe up to 250 μM throughout the Holocene profile are all consistent with a sulfide-limited system and episodically ferruginous waters. However, while sulfide accumulation in the water column was transient, if present at all, one factor likely contributing to incomplete diagenetic pyrite formation in sediments, even if sulfide was accumulating in pore waters, is the particularly elevated sedimentation rates at Lille Belt (0.66 cm/year; van Helmond et al., 2017). Specifically, elevated sedimentation rates can limit the residence time of "highly reactive" Fe minerals such as magnetite and other Fe-oxides in the sulfidic zone relative to the timescales that these minerals react with sulfide to form pyrite (Boesen and Postma, 1988; Canfield et al., 1992; Hurtgen et al., 1999; Riedinger et al., 2017).

The Mo concentrations and isotope data support the potential for anoxia with sulfide accumulation limited to sedimentary pore fluids. The Mo concentrations are elevated above detrital levels. These concentrations and the Mo isotope range of +0.18 to +1.47‰ are comparable to values observed in low oxygen basins where sulfide is restricted to sedimentary pore fluids. For example, the California Borderland Basins, which exhibit variable degrees of low oxygen conditions, have low Mo enrichments and are characterized by Mo isotope values >0.5‰ but less than seawater (Poulson Brucker et al., 2009). However, the geochemical signature most diagnostic of episodic transitions between oxygenated and likely manganous conditions is the elevated Mn observed throughout the majority of the post-ILS profile. Manganous conditions are documented in the modern Baltic Sea (up to 40 μM Mn in some studies; Dellwig et al., 2018). The water column dissolved Mn is oxidized and returned to sediments during oxygenation events related to seasonal activities or MBIs (Dellwig et al., 2010, 2018; Hermans et al., 2019). The 1.5 wt. % Mn observed in Lille Belt sediments is not as high as concentrations found in some Baltic-proper deeps (e.g., Landsort Deep, **Figure 5**), but Lille Belt Mn levels are elevated relative to sediments without episodic oscillations between manganous and oxygenated conditions (Calvert and Pedersen, 1996).

Importantly, our dataset indicates that conditions more reducing than those present today, specifically euxinia, did not exist throughout the Holocene at Lille Belt, even during the MCA and HTM. Specifically, the Fe speciation and Mo concentration proxies do not show excursions significantly above the thresholds clearly associated with euxinic conditions during any specific intervals. Further, the Mo isotope signatures remain well below that of Baltic seawater and hence provide strong evidence for Fe-Mn oxides as the main source of Mo to the sediments and hence evidence against any widespread and persistent euxinic conditions, which might otherwise have drawn down water column Mo and limited its accumulation in sediments—as has been interpreted in the Bothnian Sea during the HTM (Jilbert et al., 2015; Dijkstra et al., 2018b).

Bornholm Basin Paleoredox

The Fe and Mo sedimentary geochemical records at Bornholm Basin provide evidence for multiple paleoredox shifts associated with the Initial Littorina Sea and HTM. We first propose that the observed Fe and Mo data from the ILS at Bornholm Basin ($Mo < 25$ ppm, $\delta^{98}Mo \sim -0.5$‰, $Fe_T/Al > 0.65$, $Fe_{HR}/Fe_T > 0.38$, and $(Fe_{py}+Fe_{AVS})/Fe_{HR} > 0.7$) reflect anoxia but with hydrogen sulfide largely restricted to pore waters with only transient water column sulfide accumulation (**Figure 3**). The observed negative Mo isotope values and minor sedimentary Mo enrichments are most consistent with either: (1) molybdate to thiomolybdate transformation under conditions with low or intermittent water column sulfide or (2) sedimentary delivery of Mo via Fe and Mn-oxides and sequestration in sulfidic pore fluids—or both. Both processes yield Mo isotope fractionations up to −3‰ (Barling et al., 2001; Wasylenki et al., 2008; Goldberg et al., 2009), which could explain why our values are fractionated by nearly 2.9‰ relative to seawater. Importantly, both euxinic conditions and Fe-oxide deposition could cause enrichments in Fe_{HR}/Fe_T and Fe_T/Al relative to detrital inputs. Although the combination of $(Fe_{py}+Fe_{AVS})/Fe_{HR} > 0.7$ and elevated Fe_{HR}/Fe_T and Fe_T/Al is typically diagnostic of euxinia, the exceptional delivery of "extra" "highly reactive" Fe as Fe-oxides to the sediment could react with pore water sulfide to form pyrite and other Fe sulfides, post-depositionally elevating $(Fe_{py}+Fe_{AVS})/Fe_{HR}$. Such conditions would reflect periodic or episodic oxidation of an Fe-rich water column with delivery of oxides to organic-rich and sulfidic sediments. While post-depositional increases in Fe_T/Al and Fe_{HR}/FeT have not been documented in modern sediments, post-depositional formation of pyrite and associated increases in $(Fe_{py}+Fe_{AVS})/Fe_{HR}$ have been observed in sediments underlying oxic water columns from many localities, including the FOAM site in Long Island Sound (Canfield et al., 1992; Hardisty et al., 2018) and oxic portions of the Black Sea Shelf (Wijsman et al., 2001a), providing precedence for this possibility. While it is difficult to distinguish between these interpretations, anoxic and weakly or intermittently euxinic settings commonly overlap, thus making a single environmental assignment difficult. Indeed, the modern Bornholm Basin water column is characterized by intermittent anoxia and sulfide accumulation (**Figure 1**).

An important additional consideration for the increases in Fe_T/Al and Fe_{HR}/Fe_T specifically at the ILS-Littorina Sea Boundary at Bornholm Basin and other sub-basins is the potential for pore water Fe migration from adjacent sediments layers (Berner, 1969; Boesen and Postma, 1988). The latter is often associated with juxtapositions of organic-lean and organic-rich sediment layers, such as sapropels, and can also reflect sulfate-poor and sulfate-rich pore waters marking a transition from non-marine to marine deposition. Indeed, secondary Fe enrichments may be important at Bornholm Basin (as well as other Baltic sub-basins; e.g., Landsort Deep and Lille Belt), which contains elevated pore water dissolved Fe

concentrations in Ancylus Lake sediments that sharply decrease at the ILS boundary when the basin becomes brackish (**Figure 5**). Specifically, it is possible that the diffusion of underlying Ancylus Lake pore water Fe to the overlying sulfidic Littorina pore waters caused post-depositional Fe enrichments which are independent of water column redox conditions (Boesen and Postma, 1988; Dijkstra et al., 2018a). In order to account for upward Fe diffusing into sulfidic sediments and its potential authigenic Fe contribution to Fe_T/Al, we use Fick's first law of diffusion, as applied to sediments (Berner, 1980), to calculate Fe_{auth} at the AL-ILS transition at Bornholm Basin, Lille Belt, and Landsort Deep (Eqs 4, 5).

$$J = -\varphi D_s \frac{\Delta C}{\Delta Z}, \quad (4)$$

$$Fe_{auth} = \frac{J}{\omega \rho}, \quad (5)$$

where φ is the porosity, D_s is the diffusion coefficient for Fe^{2+} (Li and Gregory, 1974), ΔC is the change in pore water concentration across the sulfide interface, ΔZ is the depth interval from which ΔC is measured (yielding the gradient), ω is the sedimentation rate, and ρ is the sediment density. In our calculation, we model the mass flux (J) of Fe across the redox front from the Ancylus Lake to overlying sulfidic pore fluids, assuming complete precipitation of pore water dissolved Fe as Fe sulfides. The mass flux can then be used, in combination with the sediment density (ρ), porosity (φ), sedimentation rate (ω), and the minimum Al concentration among samples with observed elevated Fe_T/Al (which amplifies our calculated Fe_T/Al to the maximum extent) to estimate a potential range of authigenic Fe_T/Al enrichments. All values are given in **Table 1**.

In all cases considered, calculations suggest that the observed Fe_T/Al cannot be entirely explained by upward Fe migration into sulfidic sediments (**Figure 6**). Specifically, the calculations show the potential for similar post-depositional enrichments in Fe_T/Al at all three basins. Importantly, however, upward Fe migration cannot account for the full observed Fe_T/Al enrichments at the ILS-Littorina Sea Boundary at Bornholm Basin or Landsort Deep. We also highlight that we chose conservative values for variables in our calculations which would most likely overestimate any authigenic contributions to Fe_T/Al. The conservative nature of our estimates is highlighted by the calculated Fe_{auth} flux increases in Fe_T/Al by ~0.11 at Lille Belt, a location where no significant increases in Fe_T/Al are observed through the whole profile. This conclusion ultimately implies that a substantial portion, if not the majority, of the observed Fe_T/Al enrichments at both Bornholm Basin and Landsort Deep in the period following Ancylus Lake deposition likely result from primary water column redox dynamics and the associated Fe shuttle, thus permitting interpretation related to water column redox variations.

Further up in the profile beyond the ILS boundary, a sharp increase in TOC concurrent with an increase in Fe_T/Al, Fe_{HR}/Fe_T, Fe_{py}/Fe_{HR}, and Mo within the sapropel at Bornholm Basin at ~5 mcd (**Figure 3**) indicates a brief interval of likely intermittent euxinic conditions. The Mo concentration approaches the 36 ppm Mo found in modern Bornholm Basin sediments, which underlie an episodically euxinic water column (Mort et al., 2010) and is similar to that of some other localities with episodic euxinia (Scott and Lyons, 2012; Hardisty et al., 2018; Scholz et al., 2018). Lastly, we note that Mo isotope values for this interval—which gradually increase from the ILS within the HTM—are the most positive recorded in the entire profile (approaching +1.6‰; **Figure 3H**). These relationships and heavier Mo isotope signatures are opposite the trend expected for an interval with a prominent oxide-delivered Mo flux to the sediments, as both Mn and Fe oxides fractionate Mo isotopes to more negative values by up to 2.9‰ (Barling et al., 2001; Wasylenki et al., 2008) and 2.2‰ (Goldberg et al., 2009), respectively. A non-oxide origin for the sedimentary Mo from this interval is also supported by a lack of Mn enrichments (**Figure 4C**). Instead, the Mo isotope values are in a range consistent with sulfide concentrations <100 μM and/or sulfide accumulation for only short timescales, both which exert a

TABLE 1 | Values and associated sources for calculations shown in **Figure 6**.

	ΔC (mM)[a]	ρ (g/cm³)[b]	φ[b]	ω (cm/s)	Al_{min} (wt.%)[d]	D (cm²/s)
Lille Belt	1.70	0.75	0.8	0.66[e]	4.9	5.268×10^{-6}
Bornholm Basin	0.98	1.5	0.8	0.21[c]	7.5	5.268×10^{-6}
Landsort Deep	0.56	0.8	0.8	0.12[c]	3.8	5.268×10^{-6}

[a] ***Figure 5***.
[b] *Andrén et al., 2015a,b,c.*
[c] *Mort et al., 2010.*
[d] ***Supplementary Tables 1, 2***; *Hardisty et al., 2016.*
[e] *van Helmond et al., 2017.*

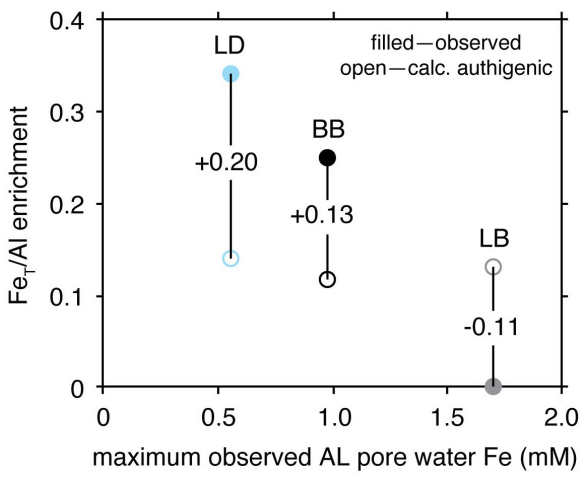

FIGURE 6 | Comparison of observed (filled) and calculated authigenic (open) Fe_T/Al enrichments at Lille Belt (LB), Bornholm Basin (BB), and Landsort Deep (LD). Observed Fe_T/Al enrichments represent the maximum from the interval directly overlying the Ancylus Lake-Littorina Sea transition relative to a detrital baseline of 0.65 (Fehr et al., 2008). Maximum pore water Fe concentrations come from the highest values generally observed in the Ancylus Lake (AL) sediments and represent ΔC in Eq. 5.

fractionation factor during only partial conversion of molybdate to tetrathiomolybdate (Azrieli-Tal et al., 2014), a condition observed in euxinic portions of the Landsort Deep today and in the recent past (Neubert et al., 2008; Noordmann et al., 2014; Hardisty et al., 2016). Alternatively, the Mo isotope values also approach the +1.6‰ that is often observed in continental margin settings with low oxygen bottom waters and sulfidic pore waters (Poulson Brucker et al., 2009). Although these independent elemental and isotopic data sets yield multiple interpretations, the combined proxies point to a system that was at least episodically anoxic with likely intermittent accumulation of water column sulfide at low levels.

Landsort Deep Paleoredox

Previously published Fe and Mo data from Landsort Deep data are distinct from those of Lille Belt and Bornholm Basin and have been interpreted to support variable degrees of euxinic conditions associated with both the HTM and MCA (**Figures 4**, **6**; Dijkstra et al., 2016; Hardisty et al., 2016; Zhou et al., 2017). Similar conditions have also been interpreted for other Baltic Proper sub-basins, albeit in the absence of Mo isotope data (e.g., Gotland Deep and Fårö Deep). Importantly, however, the Landsort Deep Mo isotope signatures are highly fractionated from seawater (**Figure 4H**), indicating some combination of two sources of Mo to the sediments: (1) low or intermittent water column sulfide accumulation inducing large Mo isotope fractionation factors during the formation of thiomolybdate species and (2) sedimentary Mo deposition with Mn- and Fe-oxides. While overlapping isotope fractionations limit our ability to isolate a specific mechanism for Mo deposition, the combined proxies point to cycles of intermittent/weak euxinia interrupted by MBIs driving dissolved Fe-Mn oxidation and oxide deposition, as is observed at Landsort Deep other Baltic-proper deeps today (Dellwig et al., 2018). Our new Fe isotope data from bulk sediment from Landsort Deep support previous indications of anoxic water column conditions as a source for the observed Fe enrichments, while new S isotope data ($\delta^{34}S_{TRS}$) for total reducible S (CRS and AVS) indicate that water column sulfide accumulation beyond transient levels may have been more limited.

The Fe isotope data range from −0.12 to +0.46‰ (**Figure 4I**), with excursions to the most negative values in intervals with elevated Fe_T/Al, Fe_{HR}/Fe_T, $(Fe_{AVS}+Fe_{py})/Fe_{HR}$, and Mo indicative of euxinia during the MCA and HTM (**Figure 4**). A previous study evaluating Fe isotope data from Gotland Deep determined an average value for sediments associated with the Baltic Ice Lake of +0.08 ± 0.13‰, which provides a baseline for the detrital flux (Fehr et al., 2008). Sedimentary Fe enrichments are attributed to shelf-to-basin transport of Fe following repeated cycles of Fe-oxide formation, dissolution in anoxic sediments, benthic fluxes from the shelf, and sequestration in anoxic environments as pyrite—i.e., the Fe shuttle (Lyons and Severmann, 2006; Severmann et al., 2008, 2010; Dellwig et al., 2010; Scholz et al., 2014b,c). The reductive dissolution of Fe oxides favors the light isotopes and results in progressive enrichment of lighter isotope signatures in benthic fluxes along shelf-to-basin transects (Severmann et al., 2010). Under euxinic conditions or events supporting large-scale oxidation of isotopically light reduced Fe (e.g., MBIs), these light Fe isotope signatures are sequestered into the sediments. While our study evaluated bulk rather than mineral-specific iron, the $(Fe_{AVS}+Fe_{py})/Fe_{HR}$ ratios support that pyrite is the largest Fe fraction during sapropel deposition. Consistent with the Fe shuttle model, the most negative Fe isotope values relative to detrital baselines are within the sapropels, which provides support—alongside that of elevated Fe_{HR}/Fe_T and Fe_T/Al—for anoxic conditions at Landsort Deep maintaining elevated Fe fluxes to the sediments. Iron isotope values for Gotland Deep show similar negative excursions during intervals with Fe_T/Al and Mo enrichments typically indicative of euxinia (Fehr et al., 2008, 2010). Importantly, the Fe isotope signatures alone cannot discern the degree to which the Fe flux at Landsort Deep was associated with syngenetic pyrite formation versus pyritization of Fe-oxide fluxes associated with either MBIs or Fe oxidation at the chemocline. Both of these processes could explain the elevated Fe_{HR}/Fe_T, $(Fe_{AVS} + Fe_{py})/Fe_{HR}$, and Mo concentrations and the highly fractionated Mo isotope values during the HTM and MCA.

We note that the most positive Fe isotope values at Landsort Deep near 0.4‰ exceed that of the Baltic detrital baseline presented by Fehr et al. (2008) of 0.08 ± 0.13‰ and are higher than the most positive values found in Littorina Sea sediments from the same study. Importantly, with the exception of one value of 0.39 ± 0.1‰ at 21.3 mcd, the most positive Fe isotope values at Landsort Deep are generally found outside of sapropel deposition. While trapping of isotopically light dissolved Fe as pyrite provides an explanation for the relatively negative Fe isotope values within the sapropels, we note that the downcore trends may be exacerbated by diagenetic trends in Fe-mineral dissolution resulting in more positive values in the intervening intervals. Specifically, the intervals outside of the sapropels have substantial pore water Fe accumulation (up to ∼250 μM; **Figure 5C**) and Fe speciation evidence most consistent with sulfide limitation in the pore waters ($Fe_{py}+Fe_{AVS}/Fe_{HR} < 0.7$; **Figure 4J**). The dissolution of Fe oxides and accumulation of dissolved Fe in sulfide-limited pore waters represents the most likely explanation for these trends. This implies the preferential release of isotopically light Fe to the pore waters, which would have the impact of distilling the remaining sedimentary Fe isotopes, such as that measured in this study, to more positive values. Ultimately, these downcore shifts between higher and lower Fe isotope values may be best explained by the combination of trapping of isotopically light dissolved Fe as sulfides during periods of euxinia or elevated pore water sulfide accumulation which are then juxtaposed against adjacent Fe-dominated intervals favoring release of isotopically light Fe to the pore waters and water column.

The S isotope data support the likelihood that much of the elevated Fe flux to the sediments during anoxic intervals was pyritized in the sediments and not the water column. The $\delta^{34}S_{TRS}$, ranging from −4.3 to +16.7‰, with an excursion to the most positive values during the HTM and MCA (**Figure 4J**), are more negative than that of sulfate in the modern Baltic Sea (+20.5‰; Böttcher and Huckriede, 1997). This relationship is consistent with negative S isotope fractionations during microbial sulfate

reduction to sulfide (Goldhaber and Kaplan, 1974; Habicht and Canfield, 2001); however, the observed $\delta^{34}S_{TRS}$ range is generally more positive than that found in euxinic basins (e.g., Black Sea; Lyons, 1997) and relative to the range observed for total reduced sulfur from a sediment core capturing the Holocene in the shallower (∼250 m), Eastern Landsort Deep (−27 to −40‰; Böttcher and Lepland, 2000). Sulfur isotope fractionations during sulfate reduction in pure cultures typically range up to 46‰ (Chambers and Trudinger, 1979) but can be as high as 70‰ (Rudnicki et al., 2001; Wortmann et al., 2001; Sim et al., 2011). The generally more positive $\delta^{34}S$ values found at Site M0063 compared to other portions of the basin and the excursion to more positive $\delta^{34}S_{TRS}$ values specifically during sapropel deposition point to non-steady steady diagenetic conditions or sulfate limitation in sedimentary pore fluids rather than changes in the $\delta^{34}S$ of Baltic Sea sulfate. This ultimately implies that the elevated $(F_{py}+Fe_{AVS})/Fe_{HR}$ ratios likely reflect processes at or below the sediment-water interface.

An increased flux of syngenetic relative to diagenetic pyrite under euxinic conditions is unlikely to explain the observed heavier pyrite $\delta^{34}S$ values during the HTM and MCA at Landsort Deep. While no sulfur isotope data exist for dissolved sulfide or reduced S fractions in the modern Landsort Deep water column, a large isotope fractionation is expected for pyrite formed in an open system (up to −60‰ in the modern Black Sea; Fry et al., 1991; Lyons, 1997). Relatively positive S isotope values are instead typically observed in diffusion-dominated pore waters where a reservoir effect (Rayleigh fractionation) allows for pore water sulfate S isotope values and associated sulfide and thus pyrite to become enriched in ^{34}S relative to seawater during sulfate reduction as sulfate concentrations become limiting at depth (Hartmann and Nielsen, 2012). Frequently these trends are associated with subsurface peaks in rates of microbial sulfate reduction at sulfate-methane transition zones at depth, with the resulting sulfide from pore water sulfate reduction, and hence pyrite, becoming relatively enriched in ^{34}S (Jørgensen et al., 2004; Borowski et al., 2013; Lin et al., 2016; Riedinger et al., 2017). At M0063, methane was detected in the uppermost sediments sampled (∼1.6 mcd), and sulfate was below detection throughout the Holocene sediments outside of samples with indications of likely seawater contamination during drilling (Egger et al., 2017). Given the shallow sulfate-methane transition zone observed today, this SMT location was likely similar or even shallower during the MCA and HTM when TOC values were as high as 8 wt. %. Under such conditions, depletions in pore water sulfate concentration coupled with increases in the S isotope signature of the sulfate and sulfide may have occurred near or at the sediment-water interface, reacting with high concentrations of "highly reactive" Fe supplied during the MCA and HTM. This would result in elevated Fe_{HR}/Fe_T and post-depositional increases in $(Fe_{py}+Fe_{AVS})/Fe_{HR}$. Alternatively, other unconstrained factors, such as an increase in sedimentation rate or an increase in sulfate reduction rate related to increased organic carbon availability are also known to decrease S isotope fractionations and hence the $\delta^{34}S_{TRS}$ compositions in sediments relative to overlying seawater (Maynard, 1980; Leavitt et al., 2013; Pasquier et al., 2017). However, if applicable, these processes still point to diagenetic origins for the variations in $\delta^{34}S_{TRS}$ in the Holocene sediments. In addition to the previously observed Mo isotope fractionations and Fe-Mn data, these new $\delta^{34}S$ data further indicate that sulfide was mostly restricted to the pore water at or below the sediment-water interface, resulting in diagenetic pyrite formation. This likelihood suggests that the MBIs and resulting oxidation of previously reduced Fe-Mn might have been the main source of Fe, Mn, and perhaps even Mo to the sediments.

Baltic Paleoredox Summary

The occurrence of ancient intervals of anoxia in the Baltic have long been known (Manheim, 1961; Suess, 1979; Sohlenius, 1996; Sohlenius et al., 1996, 2001; Sternbeck and Sohlenius, 1997, Lepland and Stevens, 1998; Sohlenius and Westman, 1998; Zillén et al., 2008), and recent studies have together constructed an increasingly detailed and quantitative understanding of the spatiotemporal variations and drivers of ancient anoxia (Mort et al., 2010; Jilbert and Slomp, 2013; Jilbert et al., 2015; Lenz et al., 2015a,b; Hardisty et al., 2016; Dijkstra et al., 2018a,b; Groeneveld et al., 2018; van Helmond et al., 2018). Our study builds on this established context by providing constraints on the specific paleoredox conditions of individual sub-basins during the Holocene. While each of the investigated sub-basins in this study show already well-known and similar changes from lacustrine to brackish—as indicated by increases in TRS/TOC ratios (Berner and Raiswell, 1984; **Figure 7A**)—and increases in TOC associated with previously established Baltic anoxic events during the HTM and MCA, our new data contribute to growing evidence that redox conditions among the sub-basins as well as between events within a given sub-basin were distinctly different. Specifically, we emphasize that, in contrast to that found in the Baltic Proper and Bothnian Sea, there is little-to-no clear evidence for ancient euxinia beyond transient events in the Lille Belt and Bornholm Basin sub-basins of the southern Baltic. This assertion is supported by comparison of $(Fe_{py}+Fe_{AVS})/Fe_{HR}$ versus Fe_{HR}/Fe_T and Mo versus TOC for these sub-basins relative to Landsort Deep (**Figures 7B,C**), which show a clear contrast.

Additionally, our study provides strong evidence against widespread euxinic conditions with stable sulfide concentrations >100 μM within even the central sub-basin, Landsort Deep—in contrast to the Bothnian Sea during the HTM. Instead, there is specific evidence that euxinia at Landsort Deep was likely isolated and limited to low and intermittent sulfide concentrations: (1) the combined Mo and Fe speciation data indicate the likelihood that water column Mo concentrations did not become depleted due to large-scale transfer to the sediment during intervals where sulfide accumulated in individual sub-basins; (2) the Mo isotope data from the Landsort Deep are all highly fractionated from seawater, which is inconsistent with conditions that were stably euxinic (**Figure 7D**); (3) S isotope evidence that diagenetic pyrite may be an important contribution to the $(Fe_{py}+Fe_{AVS})/Fe_{HR}$ trends at Landsort Deep. We note that minor seawater Mo drawdown is observed in the modern Baltic related to a combination of burial under euxinic conditions and in association with Fe-Mn-oxides (Noordmann et al., 2014), and similar conditions may have occurred previously but cannot be resolved with our proxies.

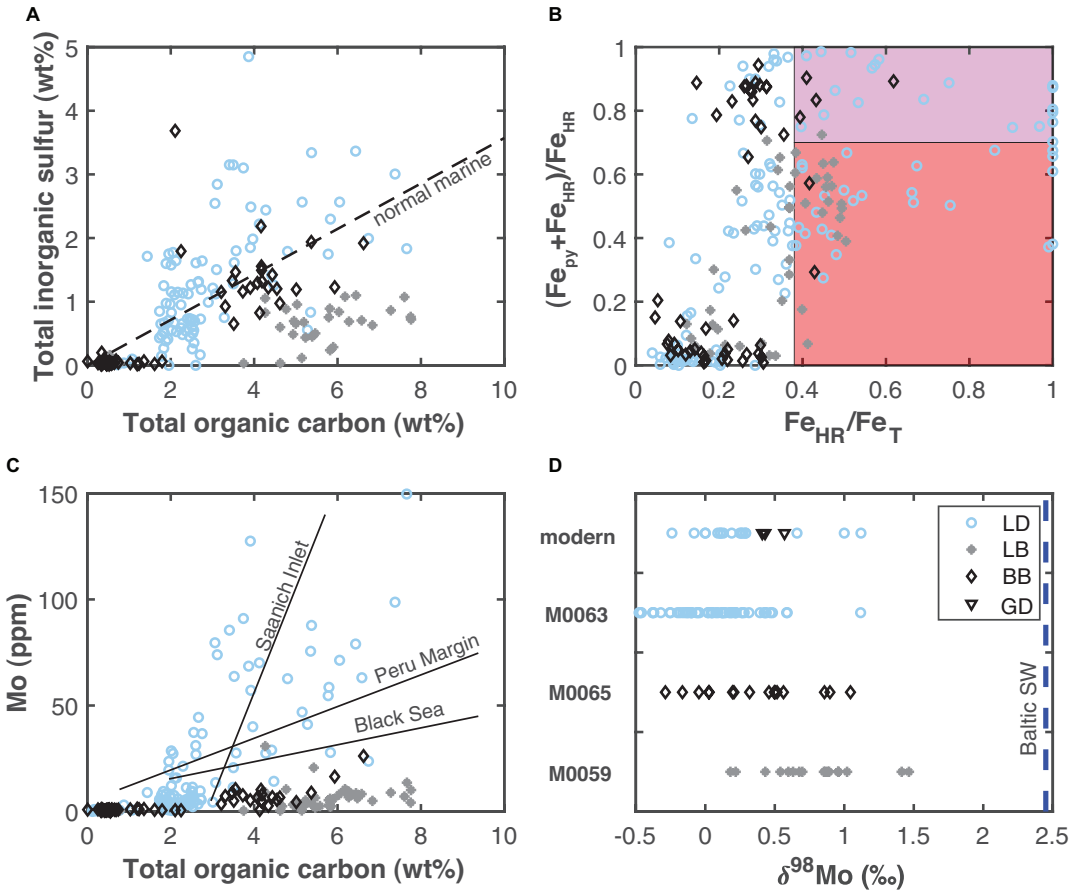

FIGURE 7 | Data comparisons between Lille Belt (LB), Bornholm Basin (BB), and Landsort Deep (LD). **(A)** Comparison of total inorganic sulfur and total organic carbon. The dashed line is the typical ratio found for marine and estuarine systems (Berner and Raiswell, 1984). **(B)** Comparison of Fe speciation. The red and purple shaded field represent that previously established for ferruginous and euxinic conditions (Raiswell et al., 2018). **(C)** Comparison of Mo and total organic carbon, with a comparison of slopes observed at modern localities with known Mo-TOC relationships (Böning et al., 2004; Algeo and Lyons, 2006; Scholz et al., 2014a). **(D)** Comparison of ranges in Mo isotope compositions for each site. The blue vertical line shows the median Mo isotope value for Baltic seawater (Noordmann et al., 2014). The modern Gotland Deep (GD) and Landsort Deep sediment Mo isotope data come from Noordmann et al. (2014) and Neubert et al. (2008).

Still, a recent study used the slope of Mo and TOC correlations from Landsort Deep sediments to suggest Mo drawdown in the Landsort Deep water column during each anoxic event (the modern, MCA, and the HTM event) (van Helmond et al., 2018), and Mo isotope comparisons between the HTM and MCA sediments suggest potentially higher sulfide and a more muted impact of Fe-Mn oxides on Mo deposition during the HTM relative to the MCA (**Figure 4H**; Hardisty et al., 2016). We note that the Mo-TOC slopes at Landsort Deep are similar to those observed in less-restricted euxinic basins (e.g., Saanich Inlet) or the Peru Margin oxygen minimum zone, where Mo deposition to sediments is largely a function of a "particulate shuttle" associated with Fe-oxide deposition as well as diffusion from seawater into underlying sediments, rather than widespread and persistent euxinic conditions (Algeo and Lyons, 2006; Algeo and Tribovillard, 2009; Hancock et al., 2019; Eroglu et al., 2020). This observation is analogous to our multi-proxy indications of Fe-Mn oxides as an important pathway for Mo deposition at Landsort Deep. Given that Mo-TOC relationships used for recognizing Mo reservoir effects are based on comparison of modern localities without major oxide-related Mo contributions to the sediments (Algeo and Lyons, 2006), the Mo-TOC slopes at Landsort Deep may not best fingerprint ancient Mo drawdown associated with euxinia.

A simplified summary of the paleoredox states established for relevant Baltic sub-basins is shown in **Figure 8**. We also note that evidence for low oxygen conditions extends beyond the MCA and HTM at both the Baltic Proper and Southern sub-basins and that redox states also appear to have been dynamic within sapropel units. Specifically, Lille Belt is characterized by anoxia with ferruginous and manganous conditions and sulfide limited to pore waters following the transition to the Littorina Sea, with no clear excursions to more reducing conditions during either the MCA or HTM. Only the HTM was studied for the Bornholm Basin, but evidence for low oxygen conditions for this interval are specific to two distinct periods of anoxia and perhaps transient euxinic conditions during the ILS and again later

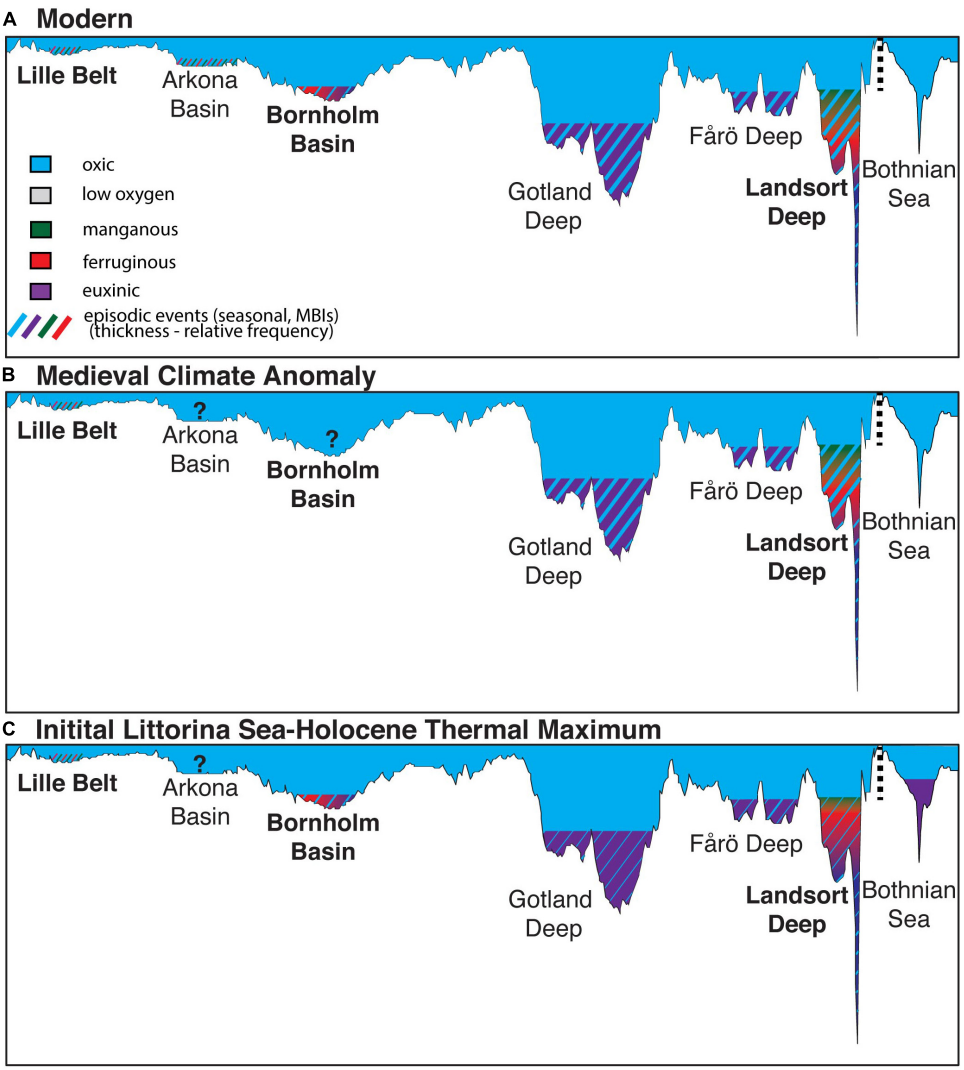

FIGURE 8 | Simplified representations of the generalized water column redox conditions during the **(A)** modern, **(B)** Medieval Climate Anomaly, and **(C)** Initial Littorina Sea and Holocene Thermal Maximum. The illustration includes interpretations from this (bold) and previous studies from Landsort Deep (Dijkstra et al., 2016), Lille Belt (van Helmond et al., 2017), Gotland Deep (van Helmond et al., 2018), Fårö Deep (van Helmond et al., 2018), and the Bothnian Sea (Jilbert et al., 2015; Dijkstra et al., 2018b). Conditions from the modern derived from multiple sources (Dellwig et al., 2012, 2018, 2019; Carstensen et al., 2014; Noordmann et al., 2014). The transect corresponds to the transect in **Figure 1**, but also includes the Bothnian Sea for comparison, with the break in the transect shown by the vertical dashed line. Paleoredox proxies discussed in the text are used to infer the specific paleoredox conditions, including: low oxygen (sediment laminations), manganous (Mn geochemistry), ferruginous (Fe geochemistry), euxinic (Fe, Mo, S geochemistry), and episodic oxygenation events (Mn and Mo geochemistry). Question marks represent basins where low oxygen conditions are recorded today, but bioturbation has been recorded in ancient sediments (Zillén et al., 2008) and insufficient or a lack of geochemical data are available to assess specific paleoredox conditions. The bathymetry matches that of today in each scenario shown, though we acknowledge that both glacio-isostatic rebound of the Baltic seafloor and different sea level would have caused this to vary from today during the ILS-LS transition and HTM.

during the HTM or Littorina Sea stage. These conditions can be further contrasted with Landsort Deep where evidence for low oxygen exists via multiple proxies throughout the Holocene, but there is additional evidence for widespread water column Fe-Mn oxide deposition and euxinia limited to low sulfide levels or transient events during both the HTM and MCA. Molybdenum and Fe_T/Al data similar to those of the Landsort Deep and typical of euxinic conditions have been observed elsewhere in the Baltic Proper (e.g., Fårö Deep and Gotland Deep), but combinations of proxies that specifically track manganous, ferruginous, and euxinic water column conditions and that differentiate pore water redox states have not been applied at those locations. While the paleoredox conditions in each sub-basin are complex, the general interpretations are consistent with the modern relationship of progressively more reducing conditions moving away from the sill and the dynamic redox conditions observed in these basins today (**Figure 1**).

Implications for Proxy Applications to Geologic Record

Our study highlights the need for proxies that constrain a range of pore water and water column redox states (manganous, ferruginous, and euxinic) in dynamic depositional and diagenetic regimes such as the Baltic Sea. This has particular importance for the recognition of diagenetic impacts on Fe speciation and the deposition of Mo, which are both widely used as paleoredox proxies. For example, recognition of diagenetic impacts on Fe speciation may be particularly important for the Precambrian and Paleozoic, when ferruginous conditions were more widespread (Sperling et al., 2015). During such intervals, caution must be taken to assure that Fe speciation indications of euxinia do not reflect ferruginous water columns overlying sediments with sulfidic pore fluids. Specifically, our combined proxies suggest that large Fe, Mn, and Mo enrichments, which today are represented by a combination of sulfides and carbonates, likely originated from deposition as Fe and Mn-oxides, perhaps via events analogous to modern MBIs. Even in Landsort Deep where euxinic conditions are observed today (Dellwig et al., 2010, 2019; Noordmann et al., 2014), we suggest that sedimentary Fe and Mo proxy values typical of euxinia likely indicate a combination of syngenetic and diagenetic origins, with MBIs oxidizing dissolved Fe and Mn that are subsequently deposited as oxides (and associated sorbed Mo). These phases are then converted to sulfides at or near the sediment-water interface. These interpretations from ancient sediments parallel direct modern observations and similar inferences for the oxidation of dissolved Mn and Fe and associated delivery of Mn and Fe-oxides and Mo to the sediments at Gotland Deep (Huckriede and Meischner, 1996; Dellwig et al., 2010, 2018; Scholz et al., 2013; Hermans et al., 2019). This Baltic model clearly differs from the controls on Fe and Mo enrichment in more restricted basins such as the Black Sea but can be distinguished through a combination of Mn enrichments and Mo and S isotope signatures tracking oxide deposition and the relative proportion of syngenetic and diagenetic pyrite formation (e.g., Planavsky et al., 2018).

CONCLUSION

We use a combination of Fe speciation and isotopes, Mo concentration and isotope data, and S isotopes to constrain paleoredox conditions in multiple sub-basins of the Baltic Sea Holocene. The records come from IODP 347 drill cores from Lille Belt, Bornholm Basin, and Landsort Deep, which together form a sill-proximal to sill-distal transect. Our goal was to assess spatiotemporal redox variations in the Baltic. The geochemical proxies provide evidence for redox heterogeneity among the locations during syndepositional events but also temporally at each individual sub-basin. Specifically, proxy evidence at Lille Belt points to sustained manganous/ferruginous conditions since the transition to the brackish Baltic Sea but with no clear excursions to more reducing conditions during the HTM or MCA, which are well-known intervals of enhanced organic carbon burial in the Baltic. Our Bornholm Basin core (which does not include the MCA) provides evidence for episodes of both ferruginous and euxinic conditions during enhanced organic carbon burial associated with HTM, but Mo isotope data limit euxinic conditions to low or transient sulfide concentrations. Lastly, euxinic conditions have already been recognized at Landsort Deep for both the MCA and HTM, but our new S isotope data are most consistent with sulfide beyond low or transient levels having been largely restricted to at or below the sediment-water interface. The Mo isotope data from all three sub-basins are highly fractionated from seawater, suggesting that particulate shuttling via Mn-Fe oxides plays a major role in the delivery of Fe, Mn, and Mo to the sediments. We also provide evidence that pyritization of these Fe-oxide fluxes during early diagenesis may be primarily responsible for increases in pyrite in some anoxic intervals. Together, paleoredox data for syndepositional events indicate more reducing conditions with increasing distance from the sill, as is observed today. Ultimately, the combination of approaches taken gives us a template for identifying specific paleoredox regimes in a highly dynamic sedimentary and diagenetic system and demonstrates the potential to identify large-scale spatial redox heterogeneity among sub-basins within a single silled basinal complex.

DATA AVAILABILITY STATEMENT

The original contributions presented in the study are included in the article/**Supplementary Material**, further inquiries can be directed to the corresponding author/s.

AUTHOR CONTRIBUTIONS

DH, NR, and TL designed the study. DH, SB, DA, and NP contributed to analytical results. DH wrote the manuscript. All authors provided feedback on the manuscript.

FUNDING

DH acknowledges funding from NSF-OCE #1923218 and a Schlanger Ocean Drilling Fellowship. DH and NR acknowledge support by the Consortium for Ocean Leadership–U.S. Science Support Program. TL acknowledges support through NASA Astrobiology Institute under Cooperative Agreement No. NNA15BB03A issued through the Science Mission Directorate.

ACKNOWLEDGMENTS

We thank the captain and crew of the Greatship Manisha and the European Consortium of Ocean Drilling.

SUPPLEMENTARY MATERIAL

The Supplementary Material for this article can be found online at: https://www.frontiersin.org/articles/10.3389/feart.2021.671401/full#supplementary-material

REFERENCES

Algeo, T. J., and Lyons, T. W. (2006). Mo–total organic carbon covariation in modern anoxic marine environments: implications for analysis of paleoredox and paleohydrographic conditions. *Paleoceanography* 21. doi: 10.1029/2004PA001112

Algeo, T. J., and Tribovillard, N. (2009). Environmental analysis of paleoceanographic systems based on molybdenum–uranium covariation. *Chem. Geol.* 268, 211–225. doi: 10.1016/j.chemgeo.2009.09.001

Andrén, T., Björck, S., Andrén, E., Conley, D., Zillén, L., and Anjar, J. (2011). *The Development of the Baltic Sea Basin during the last 130 ka, The Baltic Sea Basin*. Berlin: Springer, 75–97.

Andrén, T., Jørgensen, B. B., Cotterill, C., Green, S., Andrén, E., Ash, J., et al. (2015a). "Site M0059," in *The Expedition 347 Scientists, Proc. IODP*, eds T. Andrén, B. B. Jørgensen, C. Cotterill, and S. Green (College Station, TX: Integrated Ocean Drilling Program).

Andrén, T., Jørgensen, B. B., Cotterill, C., Green, S., Andrén, E., Ash, J., et al. (2015b). "Site M0063," in *The Expedition 347 Scientists, Proc. IODP, 347*, eds T. Andrén, B. B. Jørgensen, C. Cotterill, and S. Green (College Station, TX: Integrated Ocean Drilling Program).

Andrén, T., Jørgensen, B. B., Cotterill, C., Green, S., Andrén, E., Ash, J., et al. (2015c). "Site M0065," in *The Expedition 347 Scientists, Proc. IODP, 347*, eds T. Andrén, B. B. Jørgensen, C. Cotterill, and S. Green (College Station, TX: Integrated Ocean Drilling Program).

Ardakani, O. H., Hlohowskyj, S. R., Chappaz, A., Sanei, H., Liseroudi, M. H., and Wood, J. M. (2020). Molybdenum speciation tracking hydrocarbon migration in fine-grained sedimentary rocks. *Geochim. Cosmochim. Acta* 283, 136–148. doi: 10.1016/j.gca.2020.06.006

Arnold, G. L., Anbar, A., Barling, J., and Lyons, T. (2004). Molybdenum isotope evidence for widespread anoxia in mid-Proterozoic oceans. *Science* 304, 87–90. doi: 10.1126/science.1091785

Asael, D., Rouxel, O., Poulton, S. W., Lyons, T. W., and Bekker, A. (2018). Molybdenum record from black shales indicates oscillating atmospheric oxygen levels in the early Paleoproterozoic. *Am. J. Sci.* 318, 275–299. doi: 10.2475/03.2018.01

Asael, D., Tissot, F. L., Reinhard, C. T., Rouxel, O., Dauphas, N., Lyons, T. W., et al. (2013). Coupled molybdenum, iron and uranium stable isotopes as oceanic paleoredox proxies during the Paleoproterozoic Shunga Event. *Chem. Geol.* 362, 193–210. doi: 10.1016/j.chemgeo.2013.08.003

Azrieli-Tal, I., Matthews, A., Bar-Matthews, M., Almogi-Labin, A., Vance, D., Archer, C., et al. (2014). Evidence from molybdenum and iron isotopes and molybdenum uranium covariation for sulphidic bottom waters during Eastern Mediterranean sapropel S1 formation. *Earth Planet. Sci. Lett.* 393, 231–242. doi: 10.1016/j.epsl.2014.02.054

Barling, J., Arnold, G. L., and Anbar, A. (2001). Natural mass-dependent variations in the isotopic composition of molybdenum. *Earth Planet. Sci. Lett.* 193, 447–457. doi: 10.1016/s0012-821x(01)00514-3

Berner, R. A. (1969). Migration of iron and sulfur within anaerobic sediments during early diagenesis. *Am. J. Sci.* 267, 19–42. doi: 10.2475/ajs.267.1.19

Berner, R. A. (1980). *Early Diagenesis: A Theoretical Approach*. Princeton, NJ: Princeton University Press.

Berner, R. A., Baldwin, T., and Holdren, G. R. Jr. (1979). Authigenic iron sulfides as paleosalinit indicators. *J. Sediment. Res.* 49, 1345–1350.

Berner, R. A., and Raiswell, R. (1984). C/S method for distinguishing freshwater from marine sedimentary rocks. *Geology* 12, 365–368. doi: 10.1130/0091-7613(1984)12<365:cmfdff>2.0.co;2

Bertine, K. K., and Turekian, K. K. (1973). Molybdenum in marine deposits. *Geochim. Cosmochim. Acta* 37, 1415–1434. doi: 10.1016/0016-7037(73)90080-x

Björck, S., Andrén, T., and Jensen, J. B. (2008). An attempt to resolve the partly conflicting data and ideas on the Ancylus-Littorina transition. *Polish Geol. Institute Special Papers* 23, 21–26.

Boesen, C., and Postma, D. (1988). Pyrite formation in anoxic environments of the Baltic. *Am. J. Sci.* 288, 575–603. doi: 10.2475/ajs.288.6.575

Böning, P., Brumsack, H.-J., Böttcher, M. E., Schnetger, B., Kriete, C., Kallmeyer, J., et al. (2004). Geochemistry of Peruvian near-surface sediments. *Geochim. Cosmochim. Acta* 68, 4429–4451. doi: 10.1016/j.gca.2004.04.027

Borowski, W. S., Rodriguez, N. M., Paull, C. K., and Ussler, W. (2013). Are S-34-enriched authigenic sulfide minerals a proxy for elevated methane flux and gas hydrates in the geologic record? *Mar. Petroleum Geol.* 43, 381–395. doi: 10.1016/j.marpetgeo.2012.12.009

Böttcher, M. E., and Huckriede, H. (1997). First occurrence and stable isotope composition of authigenic gamma-MnS in the central Gotland Deep (Baltic Sea). *Mar. Geol.* 137, 201–205. doi: 10.1016/s0025-3227(96)00115-6

Böttcher, M. E., and Lepland, A. (2000). Biogeochemistry of sulfur in a sediment core from the west-central Baltic Sea: evidence from stable isotopes and pyrite textures. *J. Mar. Syst.* 25, 299–312. doi: 10.1016/s0924-7963(00)00023-3

Busigny, V., Planavsky, N. J., Jezequel, D., Crowe, S., Louvat, P., Moureau, J., et al. (2014). Iron isotopes in an Archean ocean analogue. *Geochim. Cosmochim. Acta* 133, 443–462. doi: 10.1016/j.gca.2014.03.004

Calvert, S., and Pedersen, T. (1996). Sedimentary geochemistry of manganese; implications for the environment of formation of manganiferous black shales. *Econ. Geol.* 91, 36–47.

Canfield, D., and Thamdrup, B. (2009). Towards a consistent classification scheme for geochemical environments, or, why we wish the term 'suboxic'would go away. *Geobiology* 7, 385–392. doi: 10.1111/j.1472-4669.2009.00214.x

Canfield, D. E. (1989). Reactive iron in marine sediments. *Geochim. Cosmochim. Acta* 53, 619–632. doi: 10.1016/0016-7037(89)90005-7

Canfield, D. E., and Berner, R. A. (1987). Dissolution and pyritization of magnetite in anoxie marine sediments. *Geochim. Cosmochim. Acta* 51, 645–659. doi: 10.1016/0016-7037(87)90076-7

Canfield, D. E., Lyons, T. W., and Raiswell, R. (1996). A model for iron deposition to euxinic Black Sea sediments. *Am. J. Sci.* 296, 818–834. doi: 10.2475/ajs.296.7.818

Canfield, D. E., Raiswell, R., and Bottrell, S. H. (1992). The reactivity of sedimentary iron minerals toward sulfide. *Am. J. Sci.* 292, 659–683. doi: 10.2475/ajs.292.9.659

Carstensen, J., Andersen, J. H., Gustafsson, B. G., and Conley, D. J. (2014). Deoxygenation of the Baltic Sea during the last century. *Proc. Natl. Acad. Sci. U.S.A.* 111, 5628–5633. doi: 10.1073/pnas.1323156111

Chambers, L. A., and Trudinger, P. A. (1979). Microbiological fractionation of stable sulfur isotopes: a review and critique. *Geomicrobiol. J.* 1, 249–293. doi: 10.1080/01490457909377735

Chanton, J. P., and Martens, C. S. (1985). The effects of heat and stannous chloride addition on the active distillation of acid volatile sulfide from pyrite-rich marine sediment samples. *Biogeochemistry* 1, 375–382. doi: 10.1007/bf02187379

Cline, J. D. (1969). Spectrophotometric determination of hydrogen sulfide in natural waters. *Limnol. Oceanogr.* 14, 454–458. doi: 10.4319/lo.1969.14.3.0454

Dahl, T., Chappaz, A., Hoek, J., McKenzie, C. J., Svane, S., and Canfield, D. (2017). Evidence of molybdenum association with particulate organic matter under sulfidic conditions. *Geobiology* 15, 311–323. doi: 10.1111/gbi.12220

Dahl, T. W., Chappaz, A., Fitts, J. P., and Lyons, T. W. (2013). Molybdenum reduction in a sulfidic lake: evidence from X-ray absorption fine-structure spectroscopy and implications for the Mo paleoproxy. *Geochim. Cosmochim. Acta* 103, 213–231. doi: 10.1016/j.gca.2012.10.058

Dellwig, O., Leipe, T., März, C., Glockzin, M., Pollehne, F., Schnetger, B., et al. (2010). A new particulate Mn–Fe–P-shuttle at the redoxcline of anoxic basins. *Geochim. Cosmochim. Acta* 74, 7100–7115. doi: 10.1016/j.gca.2010.09.017

Dellwig, O., Schnetger, B., Brumsack, H.-J., Grossart, H.-P., and Umlauf, L. (2012). Dissolved reactive manganese at pelagic redoxclines (part II): hydrodynamic conditions for accumulation. *J. Mar. Syst.* 90, 31–41. doi: 10.1016/j.jmarsys.2011.08.007

Dellwig, O., Schnetger, B., Meyer, D., Pollehne, F., Hausler, K., and Arz, H. W. (2018). Impact of the major baltic inflow in 2014 on manganese cycling in the gotland deep (Baltic Sea). *Front. Mar. Sci.* 5:248.

Dellwig, O., Wegwerth, A., Schnetger, B., Schulz, H., and Arz, H. W. (2019). Dissimilar behaviors of the geochemical twins W and Mo in hypoxic-euxinic marine basins. *Earth Sci. Rev.* 193, 1–23. doi: 10.1016/j.earscirev.2019.03.017

Dijkstra, N., Hagens, M., Egger, M., and Slomp, C. P. (2018a). Post-depositional formation of vivianite-type minerals alters sediment phosphorus records. *Biogeosciences* 15, 861–883. doi: 10.5194/bg-15-861-2018

Dijkstra, N., Krupinski, N. B. Q., Yamane, M., Obrochta, S. P., Miyairi, Y., Yokoyama, Y., et al. (2018b). Holocene refreshening and reoxygenation of a bothnian sea estuary led to enhanced phosphorus burial. *Estuaries Coasts* 41, 139–157. doi: 10.1007/s12237-017-0262-x

Dijkstra, N., Slomp, C. P., Behrends, T., and Expedition, S. (2016). Vivianite is a key sink for phosphorus in sediments of the Landsort Deep, an intermittently

anoxic deep basin in the Baltic Sea. *Chem. Geol.* 438, 58–72. doi: 10.1016/j.chemgeo.2016.05.025

Egger, M., Hagens, M., Sapart, C. J., Dijkstra, N., van Helmond, N. A., Mogollón, J. M., et al. (2017). Iron oxide reduction in methane-rich deep Baltic Sea sediments. *Geochim. Cosmochim. Acta* 207, 256–276. doi: 10.1016/j.gca.2017.03.019

Erickson, B. E., and Helz, G. R. (2000). Molybdenum (VI) speciation in sulfidic waters:: stability and lability of thiomolybdates. *Geochim. Cosmochim. Acta* 64, 1149–1158. doi: 10.1016/s0016-7037(99)00423-8

Eroglu, S., Scholz, F., Frank, M., and Siebert, C. (2020). Influence of particulate versus diffusive molybdenum supply mechanisms on the molybdenum isotope composition of continental margin sediments. *Geochim. Cosmochim. Acta* 273, 51–69. doi: 10.1016/j.gca.2020.01.009

Fehr, M. A., Andersson, P. S., Halenius, U., Gustafsson, O., and Mörth, C.-M. (2010). Iron enrichments and Fe isotopic compositions of surface sediments from the Gotland Deep, Baltic Sea. *Chem. Geol.* 277, 310–322. doi: 10.1016/j.chemgeo.2010.08.014

Fehr, M. A., Andersson, P. S., Hålenius, U., and Mörth, C.-M. (2008). Iron isotope variations in Holocene sediments of the Gotland Deep, Baltic Sea. *Geochim. Cosmochim. Acta* 72, 807–826. doi: 10.1016/j.gca.2007.11.033

Franck, H., Matthäus, W., and Sammler, R. (1987). Major inflows of saline water into the Baltic Sea during the present century. *Gerlands Beiträge Geophys.* 96, 517–531.

Froelich, P. N., Klinkhammer, G., Bender, M., Luedtke, N., Heath, G. R., Cullen, D., et al. (1979). Early oxidation of organic matter in pelagic sediments of the eastern equatorial Atlantic: suboxic diagenesis. *Geochim. Cosmochim. Acta* 43, 1075–1090. doi: 10.1016/0016-7037(79)90095-4

Fry, B., Jannasch, H. W., Molyneaux, S. J., Wirsen, C. O., Muramoto, J. A., and King, S. (1991). Stable isotope studies of the carbon, nitrogen and sulfur cycles in the Black Sea and the Cariaco Trench. *Oceanogr. Res. Pap.* 38, S1003–S1019.

Goldberg, T., Archer, C., Vance, D., and Poulton, S. W. (2009). Mo isotope fractionation during adsorption to Fe (oxyhydr) oxides. *Geochim. Cosmochim. Acta* 73, 6502–6516. doi: 10.1016/j.gca.2009.08.004

Goldhaber, M., and Kaplan, I. (1974). "The sulfur cycle," in *The Sea*, Vol. 5, ed. E. D. Goldberg (New York, NY: Wiley-Interscience), 569–655.

Groeneveld, J., Filipsson, H. L., Austin, W. E. N., Darling, K., McCarthy, D., Krupinski, N. B. Q., et al. (2018). Assessing proxy signatures of temperature, salinity, and hypoxia in the Baltic Sea through foraminifera-based geochemistry and faunal assemblages. *J. Micropalaeontol.* 37, 403–429. doi: 10.5194/jm-37-403-2018

Gustafsson, B. G., and Westman, P. (2002). On the causes for salinity variations in the Baltic Sea during the last 8500 years. *Paleoceanography* 17, 12–11. doi: 10.1029/2000pa000572

Habicht, K. S., and Canfield, D. E. (2001). Isotope fractionation by sulfate-reducing natural populations and the isotopic composition of sulfide in marine sediments. *Geology* 29, 555–558. doi: 10.1130/0091-7613(2001)029<0555:ifbsrn>2.0.co;2

Hancock, L. G., Hardisty, D. S., Behl, R. J., and Lyons, T. W. (2019). A multi-basin redox reconstruction for the Miocene Monterey Formation, California, USA. *Palaeogeogr. Palaeoclimatol. Palaeoecol.* 520, 114–127. doi: 10.1016/j.palaeo.2019.01.031

Hardisty, D. S., Lyons, T. W., Riedinger, N., Isson, T. T., Owens, J. D., Aller, R. C., et al. (2018). An evaluatin of sedimentary molybdenum and iron as proxies for pore fluid paleoredox conditions. *Am. J. Sci.* 318, 527–556. doi: 10.2475/05.2018.04

Hardisty, D. S., Riedinger, N., Planavsky, N. J., Asael, D., Andrén, T., Jørgensen, B. B., et al. (2016). A Holocene history of dynamic water column redox conditions in the Landsort Deep, Baltic Sea. *Am. J. Sci.* 316, 713–745. doi: 10.2475/08.2016.01

Hartmann, M., and Nielsen, H. (2012). $\delta^{34}S$ values in recent sea sediments and their significance using several sediment profiles from the western Baltic Sea. *Isotopes Environ. Health Stud.* 48, 7–32. doi: 10.1080/10256016.2012.660528

Hermans, M., Lenstra, W. K., van Helmond, N., Behrends, T., Egger, M., Seguret, M. J. M., et al. (2019). Impact of natural re-oxygenation on the sediment dynamics of manganese, iron and phosphorus in a euxinic Baltic Sea basin. *Geochim. Cosmochim. Acta* 246, 174–196. doi: 10.1016/j.gca.2018.11.033

Huckriede, H., and Meischner, D. (1996). Origin and environment of manganese-rich sediments within black-shale basins. *Geochim. Cosmochim. Acta* 60, 1399–1413. doi: 10.1016/0016-7037(96)00008-7

Hurtgen, M. T., Lyons, T. W., Ingall, E. D., and Cruse, A. M. (1999). Anomalous enrichments of iron monosulfide in euxinic marine sediments and the role of H2S in iron sulfide transformations: examples from Effingham Inlet, Orca Basin, and the Black Sea. *Am. J. Sci.* 299, 556–588. doi: 10.2475/ajs.299.7-9.556

Jilbert, T., Conley, D. J., Gustafsson, B. G., Funkey, C. P., and Slomp, C. P. (2015). Glacio-isostatic control on hypoxia in a high-latitude shelf basin. *Geology* 43, 427–430. doi: 10.1130/g36454.1

Jilbert, T., and Slomp, C. P. (2013). Rapid high-amplitude variability in Baltic Sea hypoxia during the Holocene. *Geology* 41, 1183–1186. doi: 10.1130/g34804.1

Jørgensen, B. B., Böttcher, M. E., Lüschen, H., Neretin, L. N., and Volkov, I. I. (2004). Anaerobic methane oxidation and a deep H2S sink generate isotopically heavy sulfides in Black Sea sediments. *Geochim. Cosmochim. Acta* 68, 2095–2118. doi: 10.1016/j.gca.2003.07.017

Kabel, K., Moros, M., Porsche, C., Neumann, T., Adolphi, F., Andersen, T. J., et al. (2012). Impact of climate change on the Baltic Sea ecosystem over the past 1,000 years. *Nat. Clim. Change* 2, 871–874. doi: 10.1038/nclimate1595

Kashiwabara, T., Takahashi, Y., and Tanimizu, M. (2009). A XAFS study on the mechanism of isotopic fractionation of molybdenum during its adsorption on ferromanganese oxides. *Geochem. J.* 43, e31–e36.

Kostka, J. E., and Luther, G. W. (1994). Partitioning and speciation of solid phase iron in saltmarsh sediments. *Geochim. Cosmochim. Acta* 58, 1701–1710. doi: 10.1016/0016-7037(94)90531-2

Kotthoff, U., Groeneveld, J., Ash, J. L., Fanget, A.-S., Krupinski, N. Q., Peyron, O., et al. (2017). Reconstructing Holocene temperature and salinity variations in the western Baltic Sea region: a multi-proxy comparison from the Little Belt (IODP Expedition 347, Site M0059). *Biogeosciences* 14, 5607–5632. doi: 10.5194/bg-14-5607-2017

Kowalski, N., Dellwig, O., Beck, M., Gräwe, U., Neubert, N., Nägler, T. F., et al. (2013). Pelagic molybdenum concentration anomalies and the impact of sediment resuspension on the molybdenum budget in two tidal systems of the North Sea. *Geochim. Cosmochim. Acta* 119, 198–211. doi: 10.1016/j.gca.2013.05.046

Krishnaswami, S. (1976). Authigenic transition elements in Pacific pelagic clays. *Geochim. Cosmochim. Acta* 40, 425–434. doi: 10.1016/0016-7037(76)90007-7

Leavitt, W. D., Halevy, I., Bradley, A. S., and Johnston, D. T. (2013). Influence of sulfate reduction rates on the Phanerozoic sulfur isotope record. *Proc. Natl. Acad. Sci. U.S.A.* 110, 11244–11249. doi: 10.1073/pnas.1218874110

Lenz, C., Jilbert, T., Conley, D. J., and Slomp, C. P. (2015a). Hypoxia-driven variations in iron and manganese shuttling in the Baltic Sea over the past 8 kyr. *Geochem. Geophys. Geosyst.* 16, 3754–3766. doi: 10.1002/2015gc005960

Lenz, C., Jilbert, T., Conley, D. J., Wolthers, M., and Slomp, C. P. (2015b). Are recent changes in sediment manganese sequestration in the euxinic basins of the Baltic Sea linked to the expansion of hypoxia? *Biogeosciences* 12, 4875–4894. doi: 10.5194/bg-12-4875-2015

Lepland, A., and Stevens, R. L. (1998). Manganese authigenesis in the landsort deep, Baltic Sea. *Mar. Geol.* 151, 1–25. doi: 10.1016/s0025-3227(98)00046-2

Li, Y.-H., and Gregory, S. (1974). Diffusion of ions in sea water and in deep-sea sediments. *Geochim. Cosmochim. Acta* 38, 703–714. doi: 10.1016/0016-7037(74)90145-8

Lin, Z. Y., Sun, X. M., Peckmann, J., Lu, Y., Xu, L., Strauss, H., et al. (2016). How sulfate-driven anaerobic oxidation of methane affects the sulfur isotopic composition of pyrite: a SIMS study from the South China Sea. *Chem. Geol.* 440, 26–41. doi: 10.1016/j.chemgeo.2016.07.007

Lyons, T. W. (1997). Sulfur isotopic trends and pathways of iron sulfide formation in upper Holocene sediments of the anoxic Black Sea. *Geochim. Cosmochim. Acta* 61, 3367–3382. doi: 10.1016/s0016-7037(97)00174-9

Lyons, T. W., and Kashgarian, M. (2005). Paradigm lost, paradigm found. *Oceanography* 18, 86–99. doi: 10.5670/oceanog.2005.44

Lyons, T. W., and Severmann, S. (2006). A critical look at iron paleoredox proxies: new insights from modern euxinic marine basins. *Geochim. Cosmochim. Acta* 70, 5698–5722. doi: 10.1016/j.gca.2006.08.021

Lyons, T. W., Werne, J. P., Hollander, D. J., and Murray, R. (2003). Contrasting sulfur geochemistry and Fe/Al and Mo/Al ratios across the last oxic-to-anoxic transition in the Cariaco Basin, Venezuela. *Chem. Geol.* 195, 131–157. doi: 10.1016/s0009-2541(02)00392-3

Manheim, F. T. (1961). A geochemical profile in the Baltic Sea. *Geochim. Cosmochim. Acta* 25, 52–70. doi: 10.1016/0016-7037(61)90059-x

Matthäus, W. (2006). *The History of Investigation of Salt Water Inflows Into the Baltic Sea: From Early Beginning to Recent Results*. Rostock: Institut für Meereskunde Warnemhunde.

Maynard, J. B. (1980). Sulfur isotopes of iron sulfides in Devonian-Mississippian shales of the Appalachian Basin – control by rate of sedimentation. *Am. J. Sci.* 280, 772–786. doi: 10.2475/ajs.280.8.772

Miller, C. A., Peucker-Ehrenbrink, B., Walker, B. D., and Marcantonio, F. (2011). Re-assessing the surface cycling of molybdenum and rhenium. *Geochim. Cosmochim. Acta* 75, 7146–7179. doi: 10.1016/j.gca.2011.09.005

Mohrholz, V., Naumann, M., Nausch, G., Krüger, S., and Gräwe, U. (2015). Fresh oxygen for the Baltic Sea—an exceptional saline inflow after a decade of stagnation. *J. Mar. Syst.* 148, 152–166. doi: 10.1016/j.jmarsys.2015.03.005

Morford, J. L., Martin, W. R., François, R., and Carney, C. M. (2009). A model for uranium, rhenium, and molybdenum diagenesis in marine sediments based on results from coastal locations. *Geochim. Cosmochim. Acta* 73, 2938–2960. doi: 10.1016/j.gca.2009.02.029

Morse, J. W., and Cornwell, J. C. (1987). Analysis and distribution of iron sulfide minerals in recent anoxic marine sediments. *Mar. Chem.* 22, 55–69. doi: 10.1016/0304-4203(87)90048-x

Mort, H. P., Slomp, C. P., Gustafsson, B. G., and Andersen, T. J. (2010). Phosphorus recycling and burial in Baltic Sea sediments with contrasting redox conditions. *Geochim. Cosmochim. Acta* 74, 1350–1362. doi: 10.1016/j.gca.2009.11.016

Nägler, T., Neubert, N., Böttcher, M., Dellwig, O., and Schnetger, B. (2011). Molybdenum isotope fractionation in pelagic euxinia: evidence from the modern Black and Baltic Seas. *Chem. Geol.* 289, 1–11. doi: 10.1016/j.chemgeo.2011.07.001

Nägler, T. F., Anbar, A. D., Archer, C., Goldberg, T., Gordon, G. W., Greber, N. D., et al. (2014). Proposal for an international molybdenum isotope measurement standard and data representation. *Geostandards Geoanal. Res.* 38, 149–151.

Neubert, N., Heri, A. R., Voegelin, A. R., Nägler, T. F., Schlunegger, F., and Villa, I. M. (2011). The molybdenum isotopic composition in river water: constraints from small catchments. *Earth Planet. Sci. Lett.* 304, 180–190. doi: 10.1016/j.epsl.2011.02.001

Neubert, N., Nägler, T. F., and Böttcher, M. E. (2008). Sulfidity controls molybdenum isotope fractionation into euxinic sediments: evidence from the modern Black Sea. *Geology* 36, 775–778. doi: 10.1130/g24959a.1

Ni, S., Krupinski, N. B. Q., Groeneveld, J., Fanget, A. S., Böttcher, M. E., Liu, B., et al. (2020). Holocene hydrographic variations from the baltic-North Sea transitional area (IODP Site M0059). *Paleoceanogr. Paleoclimatol.* 35, 1–20.

Noordmann, J., Weyer, S., Montoya-Pino, C., Dellwig, O., Neubert, N., Eckert, S., et al. (2014). Uranium and molybdenum isotope systematics in modern euxinic basins: case studies from the central Baltic Sea and the Kyllaren fjord (Norway). *Chem. Geol.* 396, 182–195. doi: 10.1016/j.chemgeo.2014.12.012

Papadomanolaki, N. M., Dijkstra, N., van Helmond, N. A. G. M., Hagens, M., Bauersachs, T., Kotthoff, U., et al. (2018). Controls on the onset and termination of past hypoxia in the Baltic Sea. *Palaeogeogr. Palaeoclimatol. Palaeoecol.* 490, 347–354. doi: 10.1016/j.palaeo.2017.11.012

Pasquier, V., Sansjofre, P., Rabineau, M., Revillon, S., Houghton, J., and Fike, D. A. (2017). Pyrite sulfur isotopes reveal glacial-interglacial environmental changes. *Proc. Natl. Acad. Sci. U.S.A.* 114, 5941–5945. doi: 10.1073/pnas.1618245114

Planavsky, N. J., Slack, J. F., Cannon, W. F., O'Connell, B., Isson, T. T., Asael, D., et al. (2018). Evidence for episodic oxygenation in a weakly redox-buffered deep mid-Proterozoic ocean. *Chem. Geol.* 483, 581–594. doi: 10.1016/j.chemgeo.2018.03.028

Poulson Brucker, R. L., McManus, J., Severmann, S., and Berelson, W. M. (2009). Molybdenum behavior during early diagenesis: insights from Mo isotopes. *Geochem. Geophys. Geosyst.* 10:Q06010.

Poulton, S. W., and Canfield, D. E. (2005). Development of a sequential extraction procedure for iron: implications for iron partitioning in continentally derived particulates. *Chem. Geol.* 214, 209–221. doi: 10.1016/j.chemgeo.2004.09.003

Poulton, S. W., and Canfield, D. E. (2011). Ferruginous conditions: a dominant feature of the ocean through Earth's history. *Elements* 7, 107–112. doi: 10.2113/gselements.7.2.107

Raiswell, R., Canfield, D., and Berner, R. (1994). A comparison of iron extraction methods for the determination of degree of pyritisation and the recognition of iron-limited pyrite formation. *Chem. Geol.* 111, 101–110. doi: 10.1016/0009-2541(94)90084-1

Raiswell, R., and Canfield, D. E. (1998). Sources of iron for pyrite formation in marine sediments. *Am. J. Sci.* 298, 219–245. doi: 10.2475/ajs.298.3.219

Raiswell, R., Hardisty, D., Lyons, T., Canfield, D., Owens, J., Planavsky, N., et al. (2018). The iron paleoredox proxies: a guide to the pitfalls, problems and proper practice. *Am. J. Sci.* 318, 491–526. doi: 10.2475/05.2018.03

Raiswell, R., Vu, H. P., Brinza, L., and Benning, L. G. (2010). The determination of labile Fe in ferrihydrite by ascorbic acid extraction: methodology, dissolution kinetics and loss of solubility with age and de-watering. *Chem. Geol.* 278, 70–79. doi: 10.1016/j.chemgeo.2010.09.002

Riedinger, N., Brunner, B., Krastel, S., Arnold, G. L., Wehrmann, L. M., Formolo, M. J., et al. (2017). Sulfur cycling in an iron oxide-dominated, dynamic marine depositional system: the Argentine continental margin. *Front. Earth Sci.* 5:33. doi: 10.3389/feart.2017.00033

Rudnicki, M. D., Elderfield, H., and Spiro, B. (2001). Fractionation of sulfur isotopes during bacterial sulfate reduction in deep ocean sediments at elevated temperatures. *Geochim. Cosmochim. Acta* 65, 777–789. doi: 10.1016/s0016-7037(00)00579-2

Scholz, F., Baum, M., Siebert, C., Eroglu, S., Dale, A. W., Naumann, M., et al. (2018). Sedimentary molybdenum cycling in the aftermath of seawater inflow to the intermittently euxinic Gotland Deep, Central Baltic Sea. *Chem. Geol.* 491, 27–38. doi: 10.1016/j.chemgeo.2018.04.031

Scholz, F., McManus, J., Mix, A. C., Hensen, C., and Schneider, R. R. (2014a). The impact of ocean deoxygenation on iron release from continental margin sediments. *Nat. Geosci.* 7, 433–437. doi: 10.1038/ngeo2162

Scholz, F., McManus, J., and Sommer, S. (2013). The manganese and iron shuttle in a modern euxinic basin and implications for molybdenum cycling at euxinic ocean margins. *Chem. Geol.* 355, 56–68. doi: 10.1016/j.chemgeo.2013.07.006

Scholz, F., Severmann, S., McManus, J., and Hensen, C. (2014b). Beyond the Black Sea paradigm: the sedimentary fingerprint of an open-marine iron shuttle. *Geochim. Cosmochim. Acta* 127, 368–380. doi: 10.1016/j.gca.2013.11.041

Scholz, F., Severmann, S., McManus, J., Noffke, A., Lomnitz, U., and Hensen, C. (2014c). On the isotope composition of reactive iron in marine sediments: redox shuttle versus early diagenesis. *Chem. Geol.* 389, 48–59. doi: 10.1016/j.chemgeo.2014.09.009

Scott, C., and Lyons, T. W. (2012). Contrasting molybdenum cycling and isotopic properties in euxinic versus non-euxinic sediments and sedimentary rocks: refining the paleoproxies. *Chem. Geol.* 324, 19–27. doi: 10.1016/j.chemgeo.2012.05.012

Severmann, S., Lyons, T. W., Anbar, A., McManus, J., and Gordon, G. (2008). Modern iron isotope perspective on the benthic iron shuttle and the redox evolution of ancient oceans. *Geology* 36, 487–490. doi: 10.1130/g24670a.1

Severmann, S., McManus, J., Berelson, W. M., and Hammond, D. E. (2010). The continental shelf benthic iron flux and its isotope composition. *Geochim. Cosmochim. Acta* 74, 3984–4004. doi: 10.1016/j.gca.2010.04.022

Siebert, C., Nägler, T. F., von Blanckenburg, F., and Kramers, J. D. (2003). Molybdenum isotope records as a potential new proxy for paleoceanography. *Earth Planet. Sci. Lett.* 211, 159–171. doi: 10.1016/s0012-821x(03)00189-4

Sim, M. S., Bosak, T., and Ono, S. (2011). Large sulfur isotope fractionation does not require disproportionation. *Science* 333, 74–77. doi: 10.1126/science.1205103

Sohlenius, G. (1996). Mineral magnetic properties of Late Weichselian—Holocene sediments from the northwestern Baltic Proper. *Boreas* 25, 79–88. doi: 10.1111/j.1502-3885.1996.tb00837.x

Sohlenius, G., Emeis, K.-C., Andrén, E., Andrén, T., and Kohly, A. (2001). Development of anoxia during the Holocene fresh–brackish water transition in the Baltic Sea. *Mar. Geol.* 177, 221–242. doi: 10.1016/s0025-3227(01)00174-8

Sohlenius, G., Sternbeck, J., Andrén, E., and Westman, P. (1996). Holocene history of the Baltic Sea as recorded in a sediment core from the Gotland Deep. *Mar. Geol.* 134, 183–201. doi: 10.1016/0025-3227(96)00047-3

Sohlenius, G., and Westman, P. (1998). Salinity and redox alternations in the northwestern Baltic proper during the late Holocene. *Boreas* 27, 101–114. doi: 10.1111/j.1502-3885.1998.tb00871.x

Sperling, E. A., Wolock, C. J., Morgan, A. S., Gill, B. C., Kunzmann, M., Halverson, G. P., et al. (2015). Statistical analysis of iron geochemical data suggests limited late Proterozoic oxygenation. *Nature* 523, 451–454. doi: 10.1038/nature14589

Sternbeck, J., and Sohlenius, G. (1997). Authigenic sulfide and carbonate mineral formation in Holocene sediments of the Baltic Sea. *Chem. Geol.* 135, 55–73. doi: 10.1016/s0009-2541(96)00104-0

Suess, E. (1979). Mineral phases formed in anoxic sediments by microbial decomposition of organic matter. *Geochim. Cosmochim. Acta* 43, 339–352. doi: 10.1016/0016-7037(79)90199-6

Taylor, P. D. P., Maeck, R., and Debievre, P. (1992). Determination of the absolute isotopic composition and atomic-weight of a reference sample of natural iron. *Int. J. Mass Spectr. Ion Processes* 121, 111–125. doi: 10.1016/0168-1176(92)80075-c

Taylor, S. R., and McLennan, S. M. (1995). The geochemical evolution of the continental crust. *Rev. Geophys.* 33, 241–265. doi: 10.1029/95rg00262

Teutsch, N., Schmid, M., Muller, B., Halliday, A. N., Burgmann, H., and Wehrli, B. (2009). Large iron isotope fractionation at the oxic-anoxic boundary in Lake Nyos. *Earth Planet. Sci. Lett.* 285, 52–60. doi: 10.1016/j.epsl.2009.05.044

Tossell, J. (2005). Calculating the partitioning of the isotopes of Mo between oxidic and sulfidic species in aqueous solution. *Geochim. Cosmochim. Acta* 69, 2981–2993. doi: 10.1016/j.gca.2005.01.016

van de Velde, S. J., Hylen, A., Kononets, M., Marzocchi, U., Leermakers, M., Choumiline, K., et al. (2020). Elevated sedimentary removal of Fe, Mn, and trace elements following a transient oxygenation event in the Eastern Gotland Basin, central Baltic Sea. *Geochim. Cosmochim. Acta* 271, 16–32. doi: 10.1016/j.gca.2019.11.034

van Helmond, N., Jilbert, T., and Slomp, C. P. (2018). Hypoxia in the Holocene Baltic Sea: comparing modern versus past intervals using sedimentary trace metals. *Chem. Geol.* 493, 478–490. doi: 10.1016/j.chemgeo.2018.06.028

van Helmond, N., Krupinski, N. B. Q., Lougheed, B. C., Obrochta, S. P., Andren, T., and Slomp, C. P. (2017). Seasonal hypoxia was a natural feature of the coastal zone in the Little Belt, Denmark, during the past 8 ka. *Mar. Geol.* 387, 45–57. doi: 10.1016/j.margeo.2017.03.008

van Wirdum, F., Andren, E., Wienholz, D., Koffhoff, U., Moros, M., Fanget, A.-S., et al. (2019). Middle to late holocene variations in salinity and primary productivity in the Central Baltic Sea: a multiproxy study from the landsort deep. *Front. Mar. Sci.* 6:51. doi: 10.3389/fmars.2019.00051

Vorlicek, T. P., Helz, G. R., Chappaz, A., Vue, P., Vezina, A., and Hunter, W. (2018). Molybdenum burial mechanism in sulfidic sediments: iron-sulfide pathway. *Acs Earth Space Chem.* 2, 565–576. doi: 10.1021/acsearthspacechem.8b00016

Wagner, M., Chappaz, A., and Lyons, T. W. (2017). Molybdenum speciation and burial pathway in weakly sulfidic environments: insights from XAFS. *Geochim. Cosmochim. Acta* 206, 18–29. doi: 10.1016/j.gca.2017.02.018

Warnock, J., Andren, E., Juggins, S., Lewis, J., Ryves, D. B., Andren, T., et al. (2020). A high-resolution diatom-based Middle and Late Holocene environmental history of the Little Belt region, Baltic Sea. *Boreas* 49, 1–16. doi: 10.1111/bor.12419

Wasylenki, L. E., Rolfe, B. A., Weeks, C. L., Spiro, T. G., and Anbar, A. D. (2008). Experimental investigation of the effects of temperature and ionic strength on Mo isotope fractionation during adsorption to manganese oxides. *Geochim. Cosmochim. Acta* 72, 5997–6005. doi: 10.1016/j.gca.2008.08.027

Wijsman, J. W., Middelburg, J. J., and Heip, C. H. (2001a). Reactive iron in Black Sea sediments: implications for iron cycling. *Mar. Geol.* 172, 167–180. doi: 10.1016/s0025-3227(00)00122-5

Wijsman, J. W., Middelburg, J. J., Herman, P. M., Böttcher, M. E., and Heip, C. H. (2001b). Sulfur and iron speciation in surface sediments along the northwestern margin of the Black Sea. *Mar. Chem.* 74, 261–278. doi: 10.1016/s0304-4203(01)00019-6

Wortmann, U. G., Bernasconi, S. M., and Böttcher, M. E. (2001). Hypersulfidic deep biosphere indicates extreme sulfur isotope fractionation during single-step microbial sulfate reduction. *Geology* 29, 647–650. doi: 10.1130/0091-7613(2001)029<0647:hdbies>2.0.co;2

Zerkle, A. L., Scheiderich, K., Maresca, J. A., Liermann, L. J., and Brantley, S. L. (2011). Molybdenum isotope fractionation by cyanobacterial assimilation during nitrate utilization and N_2 fixation. *Geobiology* 9, 94–106. doi: 10.1111/j.1472-4669.2010.00262.x

Zhou, X., Jenkyns, H. C., Lu, W., Hardisty, D. S., Owens, J. D., Lyons, T. W., et al. (2017). Organically bound iodine as a bottom-water redox proxy: preliminary validation and application. *Chem. Geol.* 457, 95–106. doi: 10.1016/j.chemgeo.2017.03.016

Zillén, L., Conley, D. J., Andrén, T., Andrén, E., and Björck, S. (2008). Past occurrences of hypoxia in the Baltic Sea and the role of climate variability, environmental change and human impact. *Earth Sci. Rev.* 91, 77–92. doi: 10.1016/j.earscirev.2008.10.001

Conflict of Interest: The authors declare that the research was conducted in the absence of any commercial or financial relationships that could be construed as a potential conflict of interest.